
Weight-Space Linear Recurrent Neural Networks

Roussel Desmond Nzoyem
 University of Bristol
 Bristol, UK
 rd.nzoyemngueguin@bristol.ac.uk

Nawid Keshtrand
 University of Bristol
 Bristol, UK
 yl18410@bristol.ac.uk

Idriss Tsayem
 Ecole Normale Supérieure - PSL
 Paris, FR

David A.W. Barton
 University of Bristol
 Bristol, UK

Tom Deakin
 University of Bristol
 Bristol, UK

Abstract

We introduce WARP (**W**eight-space **A**daptive **R**ecurrent **P**rediction), a simple yet powerful framework that unifies weight-space learning with linear recurrence to redefine sequence modeling. Unlike conventional recurrent neural networks (RNNs) which collapse temporal dynamics into fixed-dimensional hidden states, WARP explicitly parametrizes the hidden state as the weights of a distinct root neural network. This formulation promotes higher-resolution memory, gradient-free adaptation at test-time, and seamless integration of domain-specific physical priors. Empirical validation shows that WARP matches or surpasses state-of-the-art baselines on diverse classification tasks, spanning synthetic benchmarks to real-world datasets. Furthermore, extensive experiments across sequential image completion, dynamical system reconstruction, and multivariate time series forecasting demonstrate its expressiveness and generalization capabilities. Critically, WARP’s weight trajectories offer valuable insights into the model’s inner workings. Ablation studies confirm the architectural necessity of key components, solidifying weight-space linear RNNs as a transformative paradigm for adaptive machine intelligence.

1 Introduction

Deep sequence models consistently demonstrate limitations in generating trajectories that diverge from their training distribution [Alijani et al., 2024, Hataya et al., 2024, Graham et al., 2023]. For instance, subsets of neural ODE [Chen et al., 2018] parameters necessitate adaptation via gradient descent to maintain performance on out-of-distribution (OoD) sequences [Kassai Koupaï et al., 2024, Nzoyem et al., 2025a]. While powerful, their inherent gradient calculation cost has recently catalyzed research into gradient-free alternatives [Serrano et al., 2024, Morel et al., 2025, Hemmer and Durstewitz, 2025], essentially trading accuracy for computational efficiency. In an effort to preserve both while achieving true zero-shot adaptation, we investigate two powerful emerging paradigms: weight-space learning and linear recurrence [Rumelhart et al., 1986].

Weight-space learning — the paradigm that treats the weights and biases of a neural network as data points for another learning system [Schürholt et al., 2024] — offers unprecedented potential for extracting properties of a trained model solely from its “weights”¹. Applications span from predicting generalization error [Unterthiner et al., 2020] and recovering training data [Dupont et al., 2022] to classifying and editing implicit neural representations [De Luigi et al., 2023]. With the proliferation

¹Following the convention from [Zhou et al., 2023], we refer to the learnable parameters of the processed network as ‘weights’ (or ‘weight-space’ to indicate the space they belong to) and those of the higher-level learning system (the neural functional) as simply ‘parameters’.

State Transition & Decoding in Recurrent Neural Networks		
Standard RNNs	Linear RNNs	Weight-Space Linear RNNs
$\mathbf{h}_t = f_{\Phi}(\mathbf{h}_{t-1}, \mathbf{x}_t)$ $\mathbf{y}_t = g_{\Psi}(\mathbf{h}_t)$	$\mathbf{h}_t = A\mathbf{h}_{t-1} + B\mathbf{x}_t$ $\mathbf{y}_t = C\mathbf{h}_{t-1}$	$\theta_t = A\theta_{t-1} + B(\mathbf{x}_t - \mathbf{x}_{t-1})$ $\mathbf{y}_t = \theta_t(\tau)$

Figure 1: Conceptual comparison between various RNN architectures. Standard RNNs (e.g. [Hochreiter and Schmidhuber, 1997]) feature a non-linear transition function f_{Φ} unlike their linear counterparts (e.g. [Orvieto et al., 2023]). Our proposed WARP is a Weight-Space Linear RNN, with hidden states represented as θ_t to emphasize their view as weights of a self-decoding function (in addition to their view as tensors). In the decoding phase, $\tau = t/(T - 1)$ with T the *training* sequence length.

of model repositories such as HuggingFace and CivitAI, developing methods that effectively learn directly from weights has become increasingly vital [Kahana et al., 2024]. To date, the literature has predominantly focused on utilizing these weights as inputs and outputs to secondary models, leaving their potential as intermediate representations (e.g. latent vectors, hidden states) in end-to-end training systems unexplored.

Concurrently, **linear** Recurrent Neural Networks (RNNs) have experienced a significant resurgence, driven by their hardware-friendly nature and the resulting ease of training [Dao and Gu, 2024]. Linearity facilitates advanced parallelization capabilities [Movahedi et al., 2025], and has enabled exceptional performance on long-sequence tasks [Gu et al., 2021, Orvieto et al., 2023]. That said, recent findings question the information content of their compressed state representations [Merrill et al., 2024]. Additionally, an important body of work establishes how linear Transformers [Vaswani et al., 2017] and a particular instantiation of linear RNNs — State-Space Models (SSMs) — are fundamentally less powerful than standard RNNs [Beck et al., 2024, Deletang et al., 2023, Merrill and Sabharwal, 2023]. These strongly suggest that non-linearities are essential for the expressivity of deep sequence models.

The preceding analyses motivate our examination of **gradient-free adaptation** through the lens of weight-space linear RNNs. To harness the strengths of the aforementioned paradigms, we formulate several research questions: • *Can the weights of an auxiliary (root) neural network serve as high-resolution hidden states for linear RNNs?* • *Can the resulting architecture adapt its dynamics during inference without requiring gradient computation?* • *Can the activation functions in the root network provide sufficient non-linearity to significantly enhance the expressive capacity of such models?*

We answer all these questions in the affirmative. Specifically, our technical contributions are summarized as follows:

- (1) We propose a novel framework (WARP) for learning on sequential data, integrating weight-space features, sequence mixing via linear recurrence, and nonlinear self-decoding which enables the embedding of domain-specific inductive biases.
- (2) Following the SSM paradigm, we introduce multiple training algorithms, including an auto-regressive mode well-suited for noisy sequence. WARP demonstrates competitive or state-of-the-art performance across diverse forecasting and classification benchmarks.
- (3) We establish a comprehensive benchmark suite to evaluate various capabilities of RNNs regarding reconstruction, adaptation and memory-retention in physical systems. WARP consistently outperforms traditional RNNs, SSMs, and Transformer architectures.

2 Weight-space Adaptive Recurrent Prediction (WARP)

This section introduces WARP, a novel framework for deep sequence models that operate by directly modulating the weights of a function approximator in response to sequential inputs. We begin by establishing the problem setting, followed by WARP’s architectural and training details.

2.1 Problem Setting

Our framework addresses the canonical sequence modeling problem, wherein a computational model must establish a mapping from an input $\mathbf{x}_t \in \mathbb{R}^{D_x}$ to a corresponding output $\mathbf{y}_t \in \mathbb{R}^{D_y}$, with $t \in \{0, \dots, T-1\}$ denoting the time step index. The integer $T > 0$ represents the training sequence length, which remains invariant across all sequences within a training batch². We assume that all input sequences are sampled at the same *uniform* intervals. With B representing the batch dimension, our models establish a mapping from $\mathbb{R}^{B \times T \times D_x}$ to $\mathbb{R}^{B \times T \times D_y}$.

In the regression setting of time series **forecasting**, we have $\mathbf{y}_t \triangleq \mathbf{x}_{t+1}$, as our objective is to predict future tokens conditioned on a preceding sequence of tokens, designated as the “context” $\mathbf{x}_{<L} \triangleq \{\mathbf{x}_t\}_{t \in \{0, \dots, L-1\}}$, where L denotes the context length. Consistent with the sequence modeling literature, we desire the ability to perform auto-regressive rollouts during inference. For **classification** tasks, only the final token \mathbf{y}_{T-1} is treated as a softmax-activated logit to assign a label to the sequence.

2.2 Architecture

Unlike traditional recurrent networks that update hidden states $\mathbf{h}_t, \forall t \in \{0, \dots, T-1\}$, weight-space linear RNNs such as WARP update the flattened parameters of a *root* neural network θ_t , effectively learning a dynamics model in weight-space (see Figure 1). Specifically, we define the recurrence relation and the subsequent decoding:

$$\theta_t = A\theta_{t-1} + B\Delta\mathbf{x}_t, \quad \text{and} \quad \mathbf{y}_t = \theta_t(\tau), \quad (1)$$

where $\theta_t \in \mathbb{R}^{D_\theta}$ represents the weights of the root neural network at time step t , and $\Delta\mathbf{x}_t = \mathbf{x}_t - \mathbf{x}_{t-1}$ is the input difference. $A \in \mathbb{R}^{D_\theta \times D_\theta}$ is the state transition “weights-to-weights” matrix, and $B \in \mathbb{R}^{D_\theta \times D_x}$ the input transition “data-to-weights” matrix. Both A and B are learned during the training process defined below. To compute the output \mathbf{y}_t , the (unflattened) hidden state $\theta_t(\cdot)$ is viewed as a *non-linear* decoding function applied to the normalized training time $\tau = t/(T-1)$. Compared to other RNNs, θ_t plays both the roles of the hidden state and the decoder, effectively decoding itself. This self-decoding significantly saves on learnable parameter count.

Importantly, all hidden states can be computed efficiently thanks to the linear recurrence in Equation (1). Once materialized, all θ_t s can be decoded in parallel. This allows our model to combine the efficiency of linear recurrence with the expressivity enabled by incorporating non-linearities.

Another key aspect of our formulation is the use of input differences $\Delta\mathbf{x}_t$ rather than direct inputs \mathbf{x}_t , which is a choice Kidger et al. [2020] theoretically motivate for continuous-time RNNs. When inputs change slowly or remain constant, the weight updates become proportionally smaller, and vice-versa. WARP essentially learns to convert input inferences into neural network updates, a critical self-supervision ability for continual learning and test-time adaptation [Behrouz et al., 2024].

Root network. The root network θ_t is implemented as a multilayer perceptron (MLP) [McCulloch and Pitts, 1943] with a 1-dimensional input $\tau \in \mathbb{R}^1$, and output dimension either D_y or $2 \times D_y$ depending on whether uncertainty estimation is performed. In such settings, the network predicts in addition to a mean $\hat{\boldsymbol{\mu}}_t \in \mathbb{R}^{D_y}$, a quantity $\tilde{\boldsymbol{\sigma}}_t \in \mathbb{R}^{D_y}$ on which a positivity-enforcing function is applied to obtain an element-wise standard deviation:

$$\hat{\boldsymbol{\sigma}}_t = \max(\text{softplus}(\tilde{\boldsymbol{\sigma}}_t), \sigma_{\min}), \quad (2)$$

where σ_{\min} is a fixed positive problem-dependent lower bound for numerical stability.

Initialization. Similar to prior work [Le et al., 2015], the state transition matrix A is initialized as the identity operator $I_{D_\theta \times D_\theta}$. This emulates gradient descent and residual connections in ResNets [He et al., 2016], thereby facilitating gradient flow during backpropagation through time [Werbos, 1990]. We find that initializing the input transition matrix B as the zero matrix $\mathbf{0}_{D_\theta \times D_x}$ is useful to ensure that the sequence of weights θ_t does not diverge early on in the training. This strategic initialization also imposes a critical constraints wherein the initial hidden state θ_0 must encode semantically rich information applicable to the entire sequence.

²We note that T may be different for testing sequences. D_\bullet is the dimensionality of the sub-scripted quantity.

The initial weights θ_0 are determined by processing the first observation: $\theta_0 = \phi(\mathbf{x}_0)$, where the “initial network” ϕ is a hypernetwork [Ha et al., 2016] defined as a learnable MLP with gradually increasing width. On sequence modeling problems with fixed or mildly-varying initial conditions, we sidestep ϕ and directly learn θ_0 , which is initialized with classical techniques [Glorot and Bengio, 2010, He et al., 2015] (and subsequently flattened into a 1D vector).

2.3 Training & Inference

Analogous to SSMs [Gu et al., 2021] and subsequent linear recurrence architectures [Orvieto et al., 2023, Movahedi et al., 2025], WARP supports dual training modes: convolutional and recurrent. The former is accomplished through a systematic unrolling of the linear recurrence formulated in Equation (1), enabling the derivation of a **convolution** kernel K such that $\theta_{0:T} = K \star \Delta \mathbf{x}_{0:T}$. Comprehensive notational specifications, algorithms, and rigorous mathematical derivations are elaborated in Appendix A. In **recurrent** mode, we distinguish the auto-regressive (AR) and the relatively memory-expensive³ *non-AR* settings. The non-AR setting never sees its own predictions, making it ideal for classification tasks wherein $\theta_t(\cdot)$ only generates logits.

The recurrent AR setting is particularly advantageous for noisy forecasting tasks that necessitate accurate modeling of the sequential data distribution $p(\mathbf{y}_t | \mathbf{y}_{<t})$. To mitigate exposure bias [Schmidt, 2019], we implement teacher forcing with scheduled sampling [Bengio et al., 2015], wherein the model incorporates uncertainties by sampling $\hat{\mathbf{y}}_t \sim \mathcal{N}(\hat{\boldsymbol{\mu}}_t, \hat{\boldsymbol{\sigma}}_t^2)$ using the reparametrization trick⁴ [Kingma et al., 2013]. Selection between ground truth \mathbf{y}_t and predicted $\hat{\mathbf{y}}_t$ follows a Bernoulli distribution with probability p_{forcing} , which we define as a training hyperparameter. That said, we consistently use $\hat{\mathbf{y}}_{t-1}$ in the input difference seen in (1).

During inference on regression problems, the model operates fully auto-regressively, i.e. $p_{\text{forcing}} = 1$ within the context window, and $p_{\text{forcing}} = 0$ in the forecast window, regardless of the training mode that was used. Although other functions can be considered, our WARP models are trained by minimizing either the mean-squared error (MSE) for deterministic predictions, or the simplified negative log-likelihood (NLL) for probabilistic predictions:

$$\mathcal{L}_{\text{MSE}} \triangleq \frac{1}{T} \sum_{t=0}^{T-1} \|\mathbf{y}_t - \hat{\mathbf{y}}_t\|_2^2, \quad \mathcal{L}_{\text{NLL}} \triangleq \frac{1}{T} \sum_{t=0}^{T-1} \left(\frac{\|\mathbf{y}_t - \hat{\mathbf{y}}_t\|_2^2}{2\hat{\boldsymbol{\sigma}}_t^2} + \log \hat{\boldsymbol{\sigma}}_t \right). \quad (3)$$

As for classification problems, we use the categorical cross-entropy $\mathcal{L}_{\text{CCE}} \triangleq \sum_{c=1}^C \mathbf{y}^{(c)} \log(\hat{\mathbf{y}}_{T-1}^{(c)})$, where \mathbf{y} is the one-hot encoding of the true label class, and C is the number of classes.

3 Experiments

We evaluate WARP on real-world multivariate time series datasets, 2D images, and physical systems. Our experiments elucidate empirical questions regarding forecasting, classification, and dynamical system reconstruction and generalization. Experimental details can be found in Appendix C.

3.1 Image Completion & Time Series Forecasting

In the first part of our experiments, we focus on forecasting applied first to raster-scanned pixel-by-pixel image completion, followed by real-world electricity prediction.

Table 1: Lowest test MSE (\downarrow) and BPD (\downarrow) achieved on MNIST (Top) and CelebA (Bottom). The best along the columns is reported in **bold**, while the second-best is underlined.

MNIST	$L = 100$		$L = 300$		$L = 600$	
	MSE	BPD	MSE	BPD	MSE	BPD
GRU	0.074	<u>0.623</u>	0.054	0.573	<u>0.015</u>	0.485
LSTM	0.074	0.652	0.057	0.611	0.027	0.539
S4	<u>0.072</u>	0.640	<u>0.049</u>	<u>0.520</u>	0.019	0.406
WARP	0.071	0.615	0.042	0.516	0.014	<u>0.416</u>
CELEBA	$L = 100$		$L = 300$		$L = 600$	
	MSE	BPD	MSE	BPD	MSE	BPD
GRU	<u>0.063</u>	24.14	<u>0.048</u>	60.39	0.027	71.51
LSTM	0.064	3869	0.053	<u>7.276</u>	<u>0.032</u>	7.909
ConvCNP	0.080	<u>1.498</u>	0.100	39.91	0.132	248.1
WARP	0.051	0.052	0.040	-0.043	0.027	-0.162

³Although equal to AR in computational complexity, the recurrent non-AR setting requires more memory because like the convolutional mode, it materializes all *high-dimensional* hidden states θ_t .

⁴We remark that this sampling is not required during *inference* on smooth sequences.

Image Completion Image completion is cast as a prediction of pixel intensities. We focus on two datasets: MNIST handwritten digits [LeCun et al., 1998], and the celebrity face attributes CelebA [Liu et al., 2015]—additional image datasets are considered in Appendix D. 2D images are flattened into 1D sequences with length $T = 784$ for MNIST and $T = 1024$ for CelebA.

Following [Rush and Karamcheti, 2022], the completion task is conditioned on contexts of variable length L . We compare WARP against long-established baselines like GRU [Cho et al., 2014] and LSTM [Hochreiter and Schmidhuber, 1997]; against state-of-the-art (SoTA) SSMs like S4 [Gu et al., 2021]; and against the ConvCNP convolution-based meta-learning baseline [Gordon et al., 2020] specifically designed for image completion. All models are trained with the NLL loss in recurrent AR mode to ensure fair comparison⁵; and feature nearly the same number of learnable parameters: approximately 1.68M for MNIST, and 2M for CelebA. Results in Table 1 demonstrate the generative performance of WARP as measured by the MSE and the uncertainty-aware bits-per-dimension (BPD) metrics. We focus on the top performing models across three runs, with corresponding qualitative results — best captured by the BPD — in Appendix E.

Energy Prediction We evaluate WARP’s performance on long-range energy forecasting tasks with the Electricity Transformer Temperature (ETT) dataset [Zhou et al., 2021]. Following established methodological protocols [Nanbo et al., 2025], we utilize the open-source TSLib⁶ to obtain preprocessed data splits which we further normalize using train set statistics (additional data processing details can be found in Appendix B).

The models are tasked with predicting 96 time steps based on a context of length $L = 96$, with performance evaluated using the mean MSE across three runs. The results are shown in Figure 2, where the best along the columns is reported in a box while the second-best is underlined.

It demonstrates WARP’s superiority, achieving the best performance on all subsets except the ETTh1 subset where it ranked second. These results are particularly noteworthy given WARP’s straightforward design. Indeed, WARP offers an elegant balance between architectural simplicity and predictive power. Additional results on the ETT dataset are presented in Appendix D.

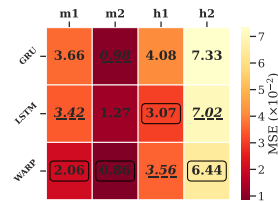


Figure 2: Heatmap of test MSEs on the ETT task.

3.2 Dynamical System Reconstruction

As our final forecasting benchmark, we evaluate WARP’s capabilities on dynamical system reconstruction (DSR) [Göring et al., 2024]. The experiments presented in this section highlight the challenge of OoD generalization to physical parameters, a research area that has recently experienced a significant surge in interest [Nzoyem et al., 2025b, Brenner et al., 2025].

We establish four DSR benchmark datasets: • (1) Mass Spring Damper (MSD) characterizes challenging damped oscillatory dynamics through physical parameters (m, k, c) , with trajectories of length $T = 256$, of which $L = 100$ serve as context; • (2) MSD-Zero is a version of MSD which varies, in addition to the significant relative scales and wide ranges of (m, k, c) , the initial condition \mathbf{x}_0 ; • (3) Lotka-Volterra (LV) is parametrized by coefficients $(\alpha, \beta, \gamma, \delta)$; • (4) SINE comprises sine curves $\tau \mapsto \sin(2\pi\tau + \varphi)$ with varying phases φ (we set $T = 16$ and $L = 1$, resulting in an initial value problem). Each test set incorporates out-of-distribution parameters, except for SINE, which primarily tests model performance under sample size constraints. Comprehensive data generation protocols for all four datasets are detailed in Appendix B. We benchmark against two established RNNs and the Time Series Transformer (TST) from HuggingFace [Jain, 2022] specialized for forecasting. We evaluate WARP in a *black-box* setting — which embeds no explicit physical knowledge in the root network — followed by the more interpretable *grey-box*.

Black-Box Setting Our results, presented in Table 2, highlight how weight-space linear RNNs consistently outperforms all baseline models across problem domains. Importantly, the standard WARP configuration which uses a root black-box MLP ranks within the top two in three out of four problem settings. We observe that TST — denoted simply as Transformer — exhibits significant performance degradation on the SINE* dataset (which comprises only 10 sequences), corroborating

⁵Additionally, the traditional dual RNN encoder-decoder approach from [Cho et al., 2014] is not used with GRU or LSTM due to the need for variable L during testing.

⁶TSLib is accessible at <https://github.com/thuml/Time-Series-Library.git>

Table 2: Average test MSE (\downarrow) and MAE (\downarrow) for dynamical system reconstruction. Best results are reported in **bold**, while the second-best are underlined. All are reported with $\times 10^{-2}$ scaling, except for SINE* with $\times 10^{-4}$. SINE* indicates that metrics are computed upon training on its ‘‘Small’’ data split. WARP-Phys indicates the variant of WARP with physical constraints in the root network.

	MSD		MSD-Zero		LV		SINE*	
	MSE	MAE	MSE	MAE	MSE	MAE	MSE	MAE
GRU	1.43 \pm 0.09	5.05	0.55 \pm 0.75	3.27 \pm 0.13	<u>5.83 \pm 0.37</u>	<u>13.1 \pm 0.42</u>	4.90 \pm 0.45	179 \pm 9.23
LSTM	1.46 \pm 0.14	5.43 \pm 0.28	0.57 \pm 0.05	3.46 \pm 0.08	6.18 \pm 0.19	13.6 \pm 0.61	9.48 \pm 0.12	248 \pm 3.45
Transformer	<u>0.34 \pm 0.12</u>	<u>2.25 \pm 0.42</u>	0.48 \pm 0.24	2.90 \pm 0.32	11.27 \pm 0.62	18.6 \pm 0.49	1728 \pm 10.8	2204 \pm 27.0
WARP	0.94 \pm 0.09	3.04 \pm 0.11	<u>0.32 \pm 0.02</u>	<u>2.59 \pm 0.07</u>	4.72 \pm 0.25	10.9 \pm 0.45	<u>2.77 \pm 0.09</u>	125 \pm 8.46
WARP-Phys	0.03 \pm 0.04	0.66 \pm 0.02	0.04 \pm 0.01	0.75 \pm 0.03	X	X	0.62 \pm 0.01	6.47 \pm 0.51

the documented limitation of Transformer models to overfit in data-scarce regimes due to their inherently high parameter complexity [Dosovitskiy et al., 2020].

Injecting Physical Bias (Grey-Box) A principal advantage of WARP is its capacity to incorporate domain-specific knowledge into the root network, exemplified on the SINE* experiment by embedding the explicit mathematical formulation $\tau \mapsto \sin(2\pi\tau + \hat{\varphi})$ in its forward pass, where $\hat{\varphi}$ is predicted by a MLP. The resulting architecture, WARP-Phys, demonstrates substantial performance improvements relative to WARP (more than one order of magnitude on MSD). Notably, the incorporation of such a powerful physical prior on SINE* underscores the value of an expressive but data-efficient initial network ϕ whose task it is to capture a representation of φ . Indeed, all models including WARP and WARP-Phys perform poorly on the extreme ‘‘Tiny’’ data split (*not* reported in Table 2). We provide additional details as ablations in Section 3.4 and Appendix D.

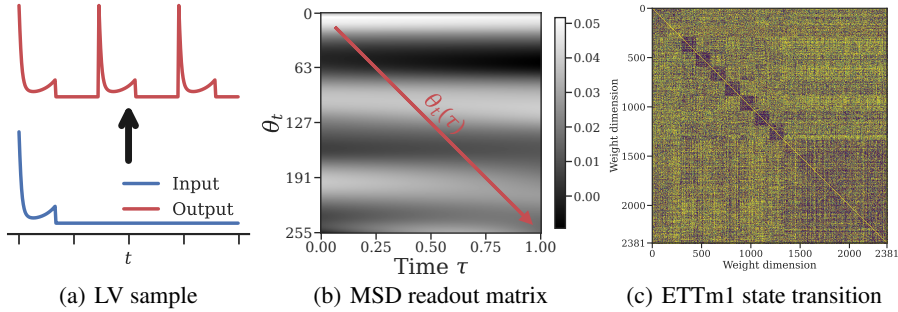


Figure 3: (a) Sample input/output sequences for the Lotka-Volterra (LV) dataset; (b) Example ‘‘readout’’ matrix on the MSD problem for all time steps t at all times τ , highlighting WARP’s diagonal decoding direction $\theta_t(\tau)$; (c) Illustration of a dense weights-to-weights A matrix.

Repeat-Copy of Physical Systems We evaluate our model’s pattern memorization capabilities on the Lotka-Volterra (LV) dataset, which constitutes a continuous analogue of the established repeat-copy benchmark [Tay et al., 2021, Orvieto et al., 2023]. To generate the output shown in red in Figure 3(a), we triplicate a concise segment of the input, delineating them by a 10-token long sequence of -1 s. In this challenging problem, WARP demonstrates superior performance relative to all baselines, with the GRU achieving the second-highest performance metrics (see Table 2). These findings suggest that the high-resolution weight-space state representation exhibits enhanced pattern retention capabilities compared to conventional methodologies. We note that this particular evaluation protocol is incompatible with the WARP-Phys variant due to the deliberate introduction of artificial discontinuities in the temporal sequences. Comprehensive analyses of additional results pertaining to this task, alongside other dynamical system reconstruction benchmarks, are presented in Appendix D.

3.3 Multivariate Time Series Classification

We now consider the classification setting. We consider six datasets from the University of East Anglia (UEA) multivariate time series classification archive (UEA-MTSCA) [Bagnall et al., 2018].

Table 3: Test-set accuracies (\uparrow) averaged over 5 training runs on the UEA classification datasets. Dataset names are abbreviated: EigenWorms (Worms), SelfRegulationSCP1 (SCP1), SelfRegulation-SCP2 (SCP2), EthanolConcentration (Ethanol), Heartbeat, MotorImagery (Motor). Best results are reported in **bold**, and the second-best are underlined.

	Worms	SCP1	SCP2	Ethanol	Heartbeat	Motor
Seq. length	17,984	896	1,152	1,751	405	3,000
# Classes	5	2	2	4	2	2
NRDE	77.2 ± 7.1	76.7 ± 5.6	48.1 ± 11.4	31.4 ± 4.5	73.9 ± 2.6	54.0 ± 7.8
NCDE	62.2 ± 3.3	80.0 ± 2.0	53.6 ± 6.2	22.0 ± 1.0	68.1 ± 5.8	51.6 ± 6.7
LRU	85.0 ± 6.2	84.5 ± 4.6	47.4 ± 4.0	29.8 ± 2.8	78.1 ± 7.6	51.9 ± 8.6
S5	<u>83.9 ± 4.1</u>	<u>87.1 ± 2.1</u>	<u>55.1 ± 3.3</u>	25.6 ± 3.5	73.9 ± 3.1	53.0 ± 3.9
Mamba	70.9 ± 15.8	80.7 ± 1.4	48.2 ± 3.9	27.9 ± 4.5	76.2 ± 3.8	47.7 ± 4.5
S6	85.0 ± 1.2	82.8 ± 2.7	49.9 ± 9.4	26.4 ± 6.4	76.5 ± 8.3	51.3 ± 4.2
Log-NCDE	82.8 ± 2.7	82.1 ± 1.4	54.0 ± 2.6	35.9 ± 6.1	74.2 ± 2.0	57.2 ± 5.6
WARP	60.98 ± 3.1	80.00 ± 2.0	57.89 ± 1.5	<u>31.65 ± 0.8</u>	<u>77.42 ± 2.2</u>	50.88 ± 2.3

The six datasets are selected and preprocessed following the criteria of known difficulty for deep sequence models and data abundance, with sequence length ranging from 405 to almost 18k [Walker et al., 2024]. Our model is compared to both discrete and continuous recurrent baselines [Morrill et al., 2021, Kidger et al., 2020, Orvieto et al., 2023, Smith et al., 2023, Walker et al., 2024, Gu and Dao, 2024]. All models are trained, validated and tested with the 70:15:15 split. Additional details on the dataset preprocessing and the baselines is provided in Appendix B.

Table 3 presents test accuracy metrics across all six benchmark datasets for WARP (trained in recurrent non-AR mode) and competing methodologies as reported in [Walker et al., 2024]. Our analysis reveals that WARP demonstrates exceptional performance across the majority of tasks, establishing new state-of-the-art benchmarks on the SCP2 dataset, and competitive second-place on two datasets: Ethanol and Heartbeat. Despite these strong results, we observe that our framework encounters performance limitations when processing extremely long sequences (specifically EigenWorms and Motor), potentially attributable to the well-documented vanishing gradient phenomenon that characteristically affects recurrent architectures [Zucchet and Orvieto, 2024]. These empirical findings substantiate WARP’s efficacy as a robust classification framework for diverse real-world time series applications.

3.4 Ablation Studies

We briefly discuss several experiments carried out to gain insights into our model. For all ablation studies, experimental protocols like training hyperparameters are presented in **Appendix C**, with detailed quantitative results in **Appendix D**.

Eliminating the root network The root network θ_t is integral to the efficacy of WARP. Although not an absolute prerequisite for the WARP-Phys variant, it nonetheless persists as a pivotal constituent of our framework. Illustratively, the omission of θ_t in favor of directly fitting φ for the SINE modeling problem results in a catastrophic degradation in model expressivity.

Root network evaluation When we fix the evaluation point τ throughout training, we observe mild degradation in the qualitative results. This emphasizes the importance of the diagonal decoding “readout” direction $\theta_t(\tau)$, illustrated for the MSD problem in Figure 3(b).

Initial network configuration Since WARP’s weight trajectories is driven by the changes in the signal and not the signal itself (see Equation (1)), it is important to have an expressive initial hypernetwork $\phi : \mathbf{x}_0 \mapsto \theta_0$, which embeds the initial tokens into suitable weight-spaces [Kidger, 2022]. Our empirical investigations reveal that sidestepping this component substantially curtails the model performance on complex synthetic benchmarks, such as MSD-Zero, and on real-world datasets, including ETT.

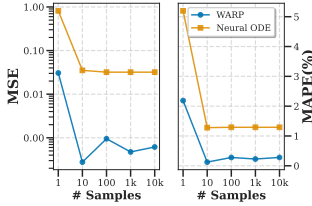


Figure 4: Data efficiency comparison on the SINE datasets.

Data efficiency With $L = 1$, the SINE benchmark is a challenging initial value problem. At equal (root) neural network parameter counts, we vary the number of training samples, and we plot MSE and MAPE test metrics for WARP and the Neural ODE [Chen et al., 2018]. The results, depicted in Figure 4, not only show improved performance across data-regimes, but they also indicate that more data is not necessarily better for WARP’s performance, suggesting potential for monotone learning [Bousquet et al., 2022].

Dense state transitions & Channel mixing The total parameter count of our model is quadratic in the root network’s dimensionality D_θ . Specifically, attempts to replace $A \in \mathbb{R}^{D_\theta \times D_\theta}$ with diagonal or low-rank approximations have resulted in remarkably less expressive models, thus solidifying its dense nature, as illustrated in Figure 3(c), as a key component of our framework.

4 Related Work

The problem of sequence modeling, long dominated by Transformers [Vaswani et al., 2017], is experiencing a renewed focus on recurrent architectures, particularly for their efficiency and unique modeling capabilities [Gu et al., 2021, De et al., 2024]. Our framework, the Weight-space Adaptive Recurrent Predictor (WARP), intersects with several active research areas.

Weight-Space Learning The concept of leveraging the weight-space of neural networks is not new; for instance, optimizers and hypernetworks inherently process weight-space features [Andrychowicz et al., 2016, Zhou et al., 2024, Ha et al., 2016], treating them as *outputs* of a learning algorithm. Other works explore weight features as *inputs* for model analysis [Unterthiner et al., 2020, Schürholt et al., 2024] or for implicitly representing data [Dupont et al., 2022]. WARP distinguishes itself by directly evolving the root network’s weights as its *intermediate* state.

Modern Linear RNNs and SSMs Linear RNNs and SSMs have re-emerged as powerful tools, largely due to their parallelizable and hardware-aware training [Yang et al., 2024, Movahedi et al., 2025], with impressive performance on long sequences. Notable architectures like S4 [Gu et al., 2021] and Linear Attention [Katharopoulos et al., 2020] have massively catalyzed recent advancements. While WARP builds on the efficiency of linear recurrence, its core innovation lies in its unique state parameterization — rather than solely on the recurrent mechanism — which includes non-linearities for improved expressivity.

Non-Linear Recurrent Mechanisms The landscape of sequence modeling is rich with innovative designs. Hybrid models like Griffin [De et al., 2024] merge recurrences with attention, while Movahedi et al. [2025] seek to compute dense linear RNNs from diagonal ones via fixed-point transformations. Frameworks like FACTS introduce structured memories [Nanbo et al., 2025]. Brain-inspired architectures [Zucchet et al., 2023, Ba et al., 2016], including time-varying decoder architectures [Jadhav et al., 2023], seek to learn evolving relationships between model inputs and outputs. WARP contributes to this evolving field by introducing a novel mechanism — viewing the RNN hidden state as the weights and biases of a time-varying root neural network — which results in non-linear self-decoding.

State and Memory in Recurrent Models A central debate revolves around the true state-tracking and memory capabilities of various recurrent architectures. While some SSMs and even Transformers face theoretical limitations in solving certain tasks [Merrill et al., 2024, Jelassi et al., 2024], improvements like incorporating negative eigenvalues in linear RNNs aim to enhance state-tracking [Grazzi et al., 2024]. Other works explicitly include neural memory modules so that surprising events are more memorable [Behrouz et al., 2024]. WARP’s use of a high-dimensional weight-space for its states is a direct attempt to provide richer “infinite-dimensional” memory capacity and more expressive temporal dynamics compared to conventional compressed state representations.

Gradient-Free Adaptation and Zero-Shot Learning Effective adaptation to out-of-distribution dynamics or in continual learning settings is a significant challenge [Green et al., 2024]. For instance,

standard Neural Ordinary Differential Equations [Chen et al., 2018] struggle with distribution shifts and need retraining or fine-tuning for adaptation [Kirchmeyer et al., 2022, Kassai Koupai et al., 2024]. With its gradient-free formulation, WARP facilitates test-time generalization, a problem explored in meta-learning frameworks like Neural Context Flows [Nzoyem et al., 2025a], through differentiable closed-form solvers [Bertinetto et al., 2018], or in-context learning [Von Oswald et al., 2023].

5 Discussion & Conclusion

5.1 Benefits

WARP demonstrates outstanding results across a multitude of data modalities, both in-distribution and out-of-distribution, as evidenced by the extensive empirical results on time series forecasting and classification we have presented (see Tables 1 to 3 and Figure 2). Additional results showcasing a 93% classification accuracy on sequential MNIST, along with ablation studies and further results on synthetic datasets are provided in Appendix D.

By letting the data directly interact with the weights as in Equation (1), WARP is able to fine-tune its weights **without gradients**, an appealing property given recent interest in test-time adaptation [Behrouz et al., 2024, Wei et al., 2022]. Additionally, WARP is the latest in the growing field of Scientific Machine Learning [Cuomo et al., 2022] that seamlessly integrates interpretable **physical knowledge** into its predictions, a feature standard RNNs have overlooked. Finally, the WARP architecture bears resemblance to synaptic plasticity in biological neural networks [Caporale and Dan, 2008]. This **neuromorphic quality** enables more biologically plausible learning dynamics.

5.2 Limitations

Some design decisions that strengthen WARP equally face limitations. We outline them below as promising avenues for future work.

Scaling to larger root networks. The size of the matrix A limits scaling to huge root neural networks. Our experiments conducted on a RTX 4080 GPU with 16GB memory could only support moderate D_θ values, leaving open the question of how expressive WARP models can become if scaled further. Future work could also explore the opposite direction, aiming to make A much smaller while preserving performance via low-rank or diagonal parametrization [Gupta et al., 2022].

Limited theoretical understanding. Although our work benefits from the theoretical underpinnings of Neural Controlled Differential Equations (CDEs) as universal approximators generalizing RNNs [Kidger, 2022], it remains mostly empirical. With the field of weight-space learning currently dominated by empirical work, more theoretical research is needed; for instance to understand and reduce the memory footprint of the matrix A as illustrated in Figure 3(c), or to enforce neuron permutation invariance [Zhou et al., 2023].

Extension to diverse tasks. Present work has focused on forecasting and classification. Future work could expand the framework to cover other forms of analyses like time series imputation or control. This could be achieved potentially through different parameterizations for the root network (e.g., CNNs, RNNs, Transformers); some of which might alleviate observed difficulties with long-range dependencies (see Table 3).

5.3 Broader Impact

While their benefits are evident from Section 5.1, malicious deployment of our self-adaptable models in scenarios they were not designed for could lead to serious adverse outcomes. Additionally, high-energy costs from high-dimensional weight-space computations could increase disparities in our field. To limit the potential for such outcomes and to improve the democratization of AI, our data and models are openly available at <https://anonymous.4open.science/r/warp>.

5.4 Conclusion

In this work, we introduced Weight-Space linear RNNs, a novel family of sequence models that operates directly within the weight-space of neural networks, offering a distinct paradigm from traditional recurrent architectures. We argue that the high-dimensional weight-space can be used for intermediate representations, resulting in infinite-dimensional RNN hidden states and high-capacity memory. Our comprehensive experiments demonstrate that our models exhibit superior expressivity and generalization capabilities, enabling a powerful form of gradient-free adaptation in response to sequential inputs, and showing exceptional abilities when integrating domain-specific knowledge from physical systems. Our framework draws intriguing parallels to neuromorphic learning principles, leading us a step further towards human-level artificial intelligence.

Acknowledgments and Disclosure of Funding

This work was supported by UK Research and Innovation grant EP/S022937/1: Interactive Artificial Intelligence, EPSRC program grant EP/R006768/1: Digital twins for improved dynamic design, EPSRC grant EP/X039137/1: The GW4 Isambard Tier-2 service for advanced computer architectures, and EPSRC grant EP/T022205/1: JADE: Joint Academic Data science Endeavour-2.

References

- Abien Fred Agarap. Deep learning using rectified linear units (relu). *arXiv preprint arXiv:1803.08375*, 2018.
- Shadi Alijani, Jamil Fayyad, and Homayoun Najjaran. Vision transformers in domain adaptation and domain generalization: a study of robustness. *Neural Computing and Applications*, 36(29):17979–18007, 2024.
- Marcin Andrychowicz, Misha Denil, Sergio Gomez, Matthew W Hoffman, David Pfau, Tom Schaul, Brendan Shillingford, and Nando De Freitas. Learning to learn by gradient descent by gradient descent. *Advances in neural information processing systems*, 29, 2016.
- Martin Arjovsky. *Out of distribution generalization in machine learning*. PhD thesis, New York University, 2020.
- Jimmy Ba, Geoffrey E Hinton, Volodymyr Mnih, Joel Z Leibo, and Catalin Ionescu. Using fast weights to attend to the recent past. *Advances in neural information processing systems*, 29, 2016.
- Anthony Bagnall, Hoang Anh Dau, Jason Lines, Michael Flynn, James Large, Aaron Bostrom, Paul Southam, and Eamonn Keogh. The uea multivariate time series classification archive, 2018. *arXiv preprint arXiv:1811.00075*, 2018.
- Maximilian Beck, Korbinian Pöppel, Markus Spanring, Andreas Auer, Oleksandra Prudnikova, Michael Kopp, Günter Klambauer, Johannes Brandstetter, and Sepp Hochreiter. xlstm: Extended long short-term memory. *arXiv preprint arXiv:2405.04517*, 2024.
- Ali Behrouz, Peilin Zhong, and Vahab Mirrokni. Titans: Learning to memorize at test time. *arXiv preprint arXiv:2501.00663*, 2024.
- Samy Bengio, Oriol Vinyals, Navdeep Jaitly, and Noam Shazeer. Scheduled sampling for sequence prediction with recurrent neural networks. *Advances in neural information processing systems*, 28, 2015.
- Luca Bertinetto, Joao F Henriques, Philip HS Torr, and Andrea Vedaldi. Meta-learning with differentiable closed-form solvers. *arXiv preprint arXiv:1805.08136*, 2018.
- Olivier J Bousquet, Amit Daniely, Haim Kaplan, Yishay Mansour, Shay Moran, and Uri Stemmer. Monotone learning. In *Conference on Learning Theory*, pages 842–866. PMLR, 2022.
- James Bradbury, Roy Frostig, Peter Hawkins, Matthew James Johnson, Chris Leary, Dougal Maclaurin, George Necula, Adam Paszke, Jake VanderPlas, Skye Wanderman-Milne, and Qiao Zhang. JAX: composable transformations of Python+NumPy programs, 2018. URL <http://github.com/google/jax>.
- Manuel Brenner, Elias Weber, Georgia Koppe, and Daniel Durstewitz. Learning interpretable hierarchical dynamical systems models from time series data. In *The Thirteenth International Conference on Learning Representations*, 2025. URL <https://openreview.net/forum?id=Vp20AxMs2s>.

- Natalia Caporale and Yang Dan. Spike timing–dependent plasticity: a hebbian learning rule. *Annu. Rev. Neurosci.*, 31(1):25–46, 2008.
- Ricky TQ Chen, Yulia Rubanova, Jesse Bettencourt, and David K Duvenaud. Neural ordinary differential equations. *Advances in neural information processing systems*, 31, 2018.
- Kyunghyun Cho, Bart Van Merriënboer, Caglar Gulcehre, Dzmitry Bahdanau, Fethi Bougares, Holger Schwenk, and Yoshua Bengio. Learning phrase representations using rnn encoder-decoder for statistical machine translation. *arXiv preprint arXiv:1406.1078*, 2014.
- Peng Cui and Jinjia Wang. Out-of-distribution (ood) detection based on deep learning: A review. *Electronics*, 11(21):3500, 2022.
- Salvatore Cuomo, Vincenzo Schiano Di Cola, Fabio Giampaolo, Gianluigi Rozza, Maziar Raissi, and Francesco Piccialli. Scientific machine learning through physics–informed neural networks: Where we are and what’s next. *Journal of Scientific Computing*, 92(3):88, 2022.
- Tri Dao and Albert Gu. Transformers are ssms: Generalized models and efficient algorithms through structured state space duality. *arXiv preprint arXiv:2405.21060*, 2024.
- Soham De, Samuel L Smith, Anushan Fernando, Aleksandar Botev, George Cristian-Muraru, Albert Gu, Ruba Haroun, Leonard Berrada, Yutian Chen, Srivatsan Srinivasan, et al. Griffin: Mixing gated linear recurrences with local attention for efficient language models. *arXiv preprint arXiv:2402.19427*, 2024.
- Luca De Luigi, Adriano Cardace, Riccardo Spezialetti, Pierluigi Zama Ramirez, Samuele Salti, and Luigi Di Stefano. Deep learning on implicit neural representations of shapes. *arXiv preprint arXiv:2302.05438*, 2023.
- DeepMind, Igor Babuschkin, Kate Baumli, Alison Bell, Surya Bhupatiraju, Jake Bruce, Peter Buchlovsky, David Budden, Trevor Cai, Aidan Clark, Ivo Danihelka, Antoine Dedieu, Claudio Fantacci, Jonathan Godwin, Chris Jones, Ross Hemsley, Tom Hennigan, Matteo Hessel, Shaobo Hou, Steven Kapturovski, Thomas Keck, Iurii Kemaev, Michael King, Markus Kunesch, Lena Martens, Hamza Merzic, Vladimir Mikulik, Tamara Norman, George Papamakarios, John Quan, Roman Ring, Francisco Ruiz, Alvaro Sanchez, Laurent Sartran, Rosalia Schneider, Eren Sezener, Stephen Spencer, Srivatsan Srinivasan, Miloš Stanojević, Wojciech Stokowiec, Luyu Wang, Guangyao Zhou, and Fabio Viola. The DeepMind JAX Ecosystem, 2020. URL <http://github.com/google-deepmind>.
- Gregoire Deletang, Anian Ruoss, Jordi Grau-Moya, Tim Genewein, Li Kevin Wenliang, Elliot Catt, Chris Cundy, Marcus Hutter, Shane Legg, Joel Veness, and Pedro A Ortega. Neural networks and the chomsky hierarchy. In *The Eleventh International Conference on Learning Representations*, 2023. URL <https://openreview.net/forum?id=WbxHAzkeQcn>.
- Alexey Dosovitskiy, Lucas Beyer, Alexander Kolesnikov, Dirk Weissenborn, Xiaohua Zhai, Thomas Unterthiner, Mostafa Dehghani, Matthias Minderer, Georg Heigold, Sylvain Gelly, et al. An image is worth 16x16 words: Transformers for image recognition at scale. *arXiv preprint arXiv:2010.11929*, 2020.
- Emilien Dupont, Hyunjik Kim, SM Eslami, Danilo Rezende, and Dan Rosenbaum. From data to functa: Your data point is a function and you can treat it like one. *arXiv preprint arXiv:2201.12204*, 2022.
- Mohamed Elsayed, Qingfeng Lan, Clare Lyle, and A. Rupam Mahmood. Weight clipping for deep continual and reinforcement learning. *RLJ*, 5:2198–2217, 2024.
- Xavier Glorot and Yoshua Bengio. Understanding the difficulty of training deep feedforward neural networks. In *Proceedings of the thirteenth international conference on artificial intelligence and statistics*, pages 249–256. JMLR Workshop and Conference Proceedings, 2010.
- Jonathan Gordon, Wessel P. Bruinsma, Andrew Y. K. Foong, James Requeima, Yann Dubois, and Richard E. Turner. Convolutional conditional neural processes. In *International Conference on Learning Representations*, 2020. URL <https://openreview.net/forum?id=Skey4eBYPS>.
- Niclas Alexander Göring, Florian Hess, Manuel Brenner, Zahra Monfared, and Daniel Durstewitz. Out-of-domain generalization in dynamical systems reconstruction. In *Forty-first International Conference on Machine Learning*, 2024. URL <https://openreview.net/forum?id=xTYIAD2NND>.
- Mark S. Graham, Petru-Daniel Tudosiu, Paul Wright, Walter Hugo Lopez Pinaya, Petteri Teikari, Ashay Patel, Jean-Marie U-King-Im, Yee H. Mah, James T. Teo, Hans Rolf Jäger, David Werring, Geraint Rees, Parashkev Nachev, Sebastien Ourselin, and M. Jorge Cardoso. Latent transformer models for out-of-distribution detection. *Medical Image Analysis*, 90:102967, 2023. ISSN 1361-8415. doi: <https://doi.org/10.1016/j.media.2023.102967>. URL <https://www.sciencedirect.com/science/article/pii/S136184152300227X>.

- Riccardo Grazi, Julien Siems, Arber Zela, Jörg KH Franke, Frank Hutter, and Massimiliano Pontil. Unlocking state-tracking in linear rnns through negative eigenvalues. *arXiv preprint arXiv:2411.12537*, 2024.
- Riku Green, Grant Stevens, Zahraa Abdallah, et al. Time-series classification for dynamic strategies in multi-step forecasting. *arXiv preprint arXiv:2402.08373*, 2024.
- Albert Gu and Tri Dao. Mamba: Linear-time sequence modeling with selective state spaces. In *First Conference on Language Modeling*, 2024. URL <https://openreview.net/forum?id=tEYskw1VY2>.
- Albert Gu, Karan Goel, and Christopher Ré. Efficiently modeling long sequences with structured state spaces. *arXiv preprint arXiv:2111.00396*, 2021.
- Ankit Gupta, Albert Gu, and Jonathan Berant. Diagonal state spaces are as effective as structured state spaces. *Advances in Neural Information Processing Systems*, 35:22982–22994, 2022.
- David Ha, Andrew Dai, and Quoc V Le. Hypernetworks. *arXiv preprint arXiv:1609.09106*, 2016.
- Ryuichiro Hataya, Kota Matsui, and Masaaki Imaizumi. Automatic domain adaptation by transformers in in-context learning. *arXiv preprint arXiv:2405.16819*, 2024.
- Kaiming He, Xiangyu Zhang, Shaoqing Ren, and Jian Sun. Delving deep into rectifiers: Surpassing human-level performance on imagenet classification. In *Proceedings of the IEEE international conference on computer vision*, pages 1026–1034, 2015.
- Kaiming He, Xiangyu Zhang, Shaoqing Ren, and Jian Sun. Deep residual learning for image recognition. In *Proceedings of the IEEE conference on computer vision and pattern recognition*, pages 770–778, 2016.
- Christoph Jürgen Hemmer and Daniel Durstewitz. True zero-shot inference of dynamical systems preserving long-term statistics. *arXiv preprint arXiv:2505.13192*, 2025.
- Sepp Hochreiter and Jürgen Schmidhuber. Long short-term memory. *Neural computation*, 9(8):1735–1780, 1997.
- Sneha Jadhav, Jianxiang Zhao, Yepeng Fan, Jingjing Li, Hao Lin, Chenggang Yan, and Minghan Chen. Time-varying sequence model. *Mathematics*, 11(2), 2023. ISSN 2227-7390. doi: 10.3390/math11020336. URL <https://www.mdpi.com/2227-7390/11/2/336>.
- Shashank Mohan Jain. Hugging face. In *Introduction to transformers for NLP: With the hugging face library and models to solve problems*, pages 51–67. Springer, 2022.
- Samy Jelassi, David Brandfonbrener, Sham M Kakade, and Eran Malach. Repeat after me: Transformers are better than state space models at copying. *arXiv preprint arXiv:2402.01032*, 2024.
- Jonathan Kahana, Eliahu Horwitz, Imri Shoval, and Yedid Hoshen. Deep linear probe generators for weight space learning. *arXiv preprint arXiv:2410.10811*, 2024.
- Armand Kassai Koupaï, Jorge Mifsut Benet, Jean-Noël Vittaut, and Patrick Gallinari. Geps: Boosting generalization in parametric pde neural solvers through adaptive conditioning. *38th Conference on Neural Information Processing Systems (NeurIPS 2024)*, 2024.
- Angelos Katharopoulos, Apoorv Vyas, Nikolaos Pappas, and François Fleuret. Transformers are rnns: Fast autoregressive transformers with linear attention. In *International conference on machine learning*, pages 5156–5165. PMLR, 2020.
- Nawid Keshtmand, Raul Santos-Rodriguez, and Jonathan Lawry. Typicality-based point ood detection with contrastive learning. In *Northern Lights Deep Learning Conference*, pages 120–129. PMLR, 2024.
- Patrick Kidger. On neural differential equations. *arXiv preprint arXiv:2202.02435*, 2022.
- Patrick Kidger and Cristian Garcia. Equinox: neural networks in JAX via callable PyTrees and filtered transformations. *Differentiable Programming workshop at Neural Information Processing Systems 2021*, 2021.
- Patrick Kidger, James Morrill, James Foster, and Terry Lyons. Neural controlled differential equations for irregular time series. *Advances in Neural Information Processing Systems*, 33:6696–6707, 2020.
- Diederik P Kingma, Max Welling, et al. Auto-encoding variational bayes, 2013.

- Matthieu Kirchmeyer, Yuan Yin, Jérémie Donà, Nicolas Baskiotis, Alain Rakotomamonjy, and Patrick Gallinari. Generalizing to new physical systems via context-informed dynamics model. In *International Conference on Machine Learning*, pages 11283–11301. PMLR, 2022.
- Quoc V Le, Navdeep Jaitly, and Geoffrey E Hinton. A simple way to initialize recurrent networks of rectified linear units. *arXiv preprint arXiv:1504.00941*, 2015.
- Yann LeCun, Léon Bottou, Yoshua Bengio, and Patrick Haffner. Gradient-based learning applied to document recognition. *Proceedings of the IEEE*, 86(11):2278–2324, 1998.
- Ziwei Liu, Ping Luo, Xiaogang Wang, and Xiaoou Tang. Deep learning face attributes in the wild. In *Proceedings of International Conference on Computer Vision (ICCV)*, December 2015.
- Warren S McCulloch and Walter Pitts. A logical calculus of the ideas immanent in nervous activity. *The bulletin of mathematical biophysics*, 5:115–133, 1943.
- William Merrill and Ashish Sabharwal. The parallelism tradeoff: Limitations of log-precision transformers. *Transactions of the Association for Computational Linguistics*, 11:531–545, 2023.
- William Merrill, Jackson Petty, and Ashish Sabharwal. The illusion of state in state-space models. In *Forty-first International Conference on Machine Learning*, 2024. URL <https://openreview.net/forum?id=QZgo9JZpLq>.
- Rudy Morel, Jiequn Han, and Edouard Oyallon. Disco: learning to discover an evolution operator for multi-physics-agnostic prediction. *arXiv preprint arXiv:2504.19496*, 2025.
- James Morrill, Cristopher Salvi, Patrick Kidger, and James Foster. Neural rough differential equations for long time series. In *International Conference on Machine Learning*, pages 7829–7838. PMLR, 2021.
- Sajad Movahedi, Felix Sarnthein, Nicola Muca Cirone, and Antonio Orvieto. Fixed-point rnns: From diagonal to dense in a few iterations. *arXiv preprint arXiv:2503.10799*, 2025.
- Li Nanbo, Firas Laakom, Yucheng XU, Wenyi Wang, and Jürgen Schmidhuber. FACTS: A factored state-space framework for world modelling. In *The Thirteenth International Conference on Learning Representations*, 2025. URL <https://openreview.net/forum?id=dmCGjPFVhF>.
- Roussel Desmond Nzoyem and Stephane Labbe. Fracturation de floes de glace par percussion dans un modèle granulaire. *GitHub*, 2021. URL <https://github.com/ddrous/ice-floes/blob/master/reports/internship/out/main.pdf>.
- Roussel Desmond Nzoyem, David AW Barton, and Tom Deakin. Extending contextual self-modulation: Meta-learning across modalities, task dimensionalities, and data regimes. *arXiv preprint arXiv:2410.01655*, 2024.
- Roussel Desmond Nzoyem, David A.W. Barton, and Tom Deakin. Neural context flows for meta-learning of dynamical systems. In *The Thirteenth International Conference on Learning Representations*, 2025a. URL <https://openreview.net/forum?id=8vzMLo8LDN>.
- Roussel Desmond Nzoyem, David AW Barton, and Tom Deakin. Towards foundational models for dynamical system reconstruction: Hierarchical meta-learning via mixture of experts. *arXiv preprint arXiv:2502.05335*, 2025b.
- Antonio Orvieto, Samuel L Smith, Albert Gu, Anushan Fernando, Caglar Gulcehre, Razvan Pascanu, and Soham De. Resurrecting recurrent neural networks for long sequences. In *International Conference on Machine Learning*, pages 26670–26698. PMLR, 2023.
- Adam Paszke, Sam Gross, Soumith Chintala, Gregory Chanan, Edward Yang, Zachary DeVito, Zeming Lin, Alban Desmaison, Luca Antiga, and Adam Lerer. Automatic differentiation in pytorch. 2017.
- Prajit Ramachandran, Barret Zoph, and Quoc V. Le. Swish: a self-gated activation function. *arXiv: Neural and Evolutionary Computing*, 2017. URL <https://api.semanticscholar.org/CorpusID:196158220>.
- David E Rumelhart, Paul Smolensky, James L McClelland, and G Hinton. Sequential thought processes in pdp models. *Parallel distributed processing: explorations in the microstructures of cognition*, 2:3–57, 1986.
- T Konstantin Rusch and Daniela Rus. Oscillatory state-space models. *arXiv preprint arXiv:2410.03943*, 2024.
- Alexander Rush and Sidd Karamcheti. The annotated s4. In *ICLR Blog Track*, 2022. URL <https://iclr-blog-track.github.io/2022/03/25/annotated-s4/>. <https://iclr-blog-track.github.io/2022/03/25/annotated-s4/>.

- Florian Schmidt. Generalization in generation: A closer look at exposure bias. *arXiv preprint arXiv:1910.00292*, 2019.
- Konstantin Schürholt, Michael W Mahoney, and Damian Borth. Towards scalable and versatile weight space learning. *arXiv preprint arXiv:2406.09997*, 2024.
- Louis Serrano, Armand Kassaï Koupai, Thomas X Wang, Pierre Erbacher, and Patrick Gallinari. Zebra: In-context and generative pretraining for solving parametric pdes. *arXiv preprint arXiv:2410.03437*, 2024.
- Jimmy T.H. Smith, Andrew Warrington, and Scott Linderman. Simplified state space layers for sequence modeling. In *The Eleventh International Conference on Learning Representations*, 2023. URL <https://openreview.net/forum?id=Ai8Hw3AXqks>.
- Yi Tay, Mostafa Dehghani, Samira Abnar, Yikang Shen, Dara Bahri, Philip Pham, Jinfeng Rao, Liu Yang, Sebastian Ruder, and Donald Metzler. Long range arena : A benchmark for efficient transformers. In *International Conference on Learning Representations*, 2021. URL <https://openreview.net/forum?id=qVyeW-grC2k>.
- Emmanuel Trélat. *Contrôle optimal: théorie & applications*, volume 36. 2005.
- Thomas Unterthiner, Daniel Keysers, Sylvain Gelly, Olivier Bousquet, and Ilya Tolstikhin. Predicting neural network accuracy from weights. *arXiv preprint arXiv:2002.11448*, 2020.
- Ashish Vaswani, Noam Shazeer, Niki Parmar, Jakob Uszkoreit, Llion Jones, Aidan N Gomez, Łukasz Kaiser, and Illia Polosukhin. Attention is all you need. *Advances in neural information processing systems*, 30, 2017.
- Pauli Virtanen, Ralf Gommers, Travis E. Oliphant, Matt Haberland, Tyler Reddy, David Cournapeau, Evgeni Burovski, Pearu Peterson, Warren Weckesser, Jonathan Bright, Stéfan J. van der Walt, Matthew Brett, Joshua Wilson, K. Jarrod Millman, Nikolay Mayorov, Andrew R. J. Nelson, Eric Jones, Robert Kern, Eric Larson, C J Carey, İlhan Polat, Yu Feng, Eric W. Moore, Jake VanderPlas, Denis Laxalde, Josef Perktold, Robert Cimrman, Ian Henriksen, E. A. Quintero, Charles R. Harris, Anne M. Archibald, Antônio H. Ribeiro, Fabian Pedregosa, Paul van Mulbregt, and SciPy 1.0 Contributors. SciPy 1.0: Fundamental Algorithms for Scientific Computing in Python. *Nature Methods*, 17:261–272, 2020. doi: 10.1038/s41592-019-0686-2.
- Johannes Von Oswald, Eyvind Niklasson, Ettore Randazzo, João Sacramento, Alexander Mordvintsev, Andrey Zhmoginov, and Max Vladymyrov. Transformers learn in-context by gradient descent. In *International Conference on Machine Learning*, pages 35151–35174. PMLR, 2023.
- Benjamin Walker, Andrew D McLeod, Tiexin Qin, Yichuan Cheng, Haoliang Li, and Terry Lyons. Log neural controlled differential equations: The lie brackets make a difference. *arXiv preprint arXiv:2402.18512*, 2024.
- Jason Wei, Xuezhi Wang, Dale Schuurmans, Maarten Bosma, Fei Xia, Ed Chi, Quoc V Le, Denny Zhou, et al. Chain-of-thought prompting elicits reasoning in large language models. *Advances in neural information processing systems*, 35:24824–24837, 2022.
- Paul J Werbos. Backpropagation through time: what it does and how to do it. *Proceedings of the IEEE*, 78(10): 1550–1560, 1990.
- Han Xiao, Kashif Rasul, and Roland Vollgraf. Fashion-mnist: a novel image dataset for benchmarking machine learning algorithms, 2017.
- Songlin Yang, Bailin Wang, Yu Zhang, Yikang Shen, and Yoon Kim. Parallelizing linear transformers with the delta rule over sequence length. In *The Thirty-eighth Annual Conference on Neural Information Processing Systems*, 2024. URL <https://openreview.net/forum?id=y8Rm4VNRPH>.
- Allan Zhou, Kaien Yang, Yiding Jiang, Kaylee Burns, Winnie Xu, Samuel Sokota, J Zico Kolter, and Chelsea Finn. Neural functional transformers. *Advances in neural information processing systems*, 36:77485–77502, 2023.
- Allan Zhou, Chelsea Finn, and James Harrison. Universal neural functionals. *arXiv preprint arXiv:2402.05232*, 2024.
- Haoyi Zhou, Shanghang Zhang, Jieqi Peng, Shuai Zhang, Jianxin Li, Hui Xiong, and Wancai Zhang. Informer: Beyond efficient transformer for long sequence time-series forecasting. In *Proceedings of the AAAI conference on artificial intelligence*, volume 35, pages 11106–11115, 2021.
- Jiachen Zhu, Xinlei Chen, Kaiming He, Yann LeCun, and Zhuang Liu. Transformers without normalization. In *Proceedings of the IEEE/CVF Conference on Computer Vision and Pattern Recognition (CVPR)*, 2025.

- Juntang Zhuang, Tommy Tang, Yifan Ding, Sekhar C Tatikonda, Nicha Dvornek, Xenophon Papademetris, and James Duncan. Adabelief optimizer: Adapting stepsizes by the belief in observed gradients. *Advances in neural information processing systems*, 33:18795–18806, 2020.
- Luisa Zintgraf, Kyriacos Shiarli, Vitaly Kurin, Katja Hofmann, and Shimon Whiteson. Fast context adaptation via meta-learning. In *International Conference on Machine Learning*, pages 7693–7702. PMLR, 2019.
- Nicolas Zucchet and Antonio Orvieto. Recurrent neural networks: vanishing and exploding gradients are not the end of the story. In *The Thirty-eighth Annual Conference on Neural Information Processing Systems, 2024*. URL <https://openreview.net/forum?id=46Jr4sgTWa>.
- Nicolas Zucchet, Robert Meier, Simon Schug, Asier Mujika, and Joao Sacramento. Online learning of long-range dependencies. In *Thirty-seventh Conference on Neural Information Processing Systems, 2023*. URL <https://openreview.net/forum?id=Wa1GGPqjUn>.

Weight-Space Linear Recurrent Neural Networks

Supplementary Material

A	Methodology	17
A.1	Motivation	17
A.2	Training Algorithms	17
A.3	Implementation Details	19
B	Datasets, Baselines & Metrics	21
B.1	Datasets	21
B.2	Baselines	22
B.3	Metrics	23
C	Experimental Details	25
C.1	Image Completion	25
C.2	Image classification	26
C.3	Energy forecasting	26
C.4	Dynamical System Reconstruction	26
C.5	Time Series Classification	27
D	Additional Results	28
D.1	2D Image Experiments	28
D.2	Spirals & Neural CDEs	28
D.3	Dynamics Reconstruction	28
D.4	Extended Ablation Insights	29
E	Visualizations	31

A Methodology

A.1 Motivation

The main motivation behind WARP (Weight-space Adaptive Recurrent Prediction) is gradient-free adaptation to out-of-distribution (OoD) settings. Relative to OoD *detection* which has always been a central problem in machine learning spanning decades of research interest [Cui and Wang, 2022, Keshtmand et al., 2024], OoD *adaptation* is a recent but growing field rich in new and stimulating ideas [Arjovsky, 2020, Nzoyem et al., 2025a]. WARP mimics the dynamics of gradient descent as observed through a projection of a 4898-dimensional space into a 2-dimensional PCA space in Figure 5(a). This offers a promising avenue for OoD adaptation with minimal cost.

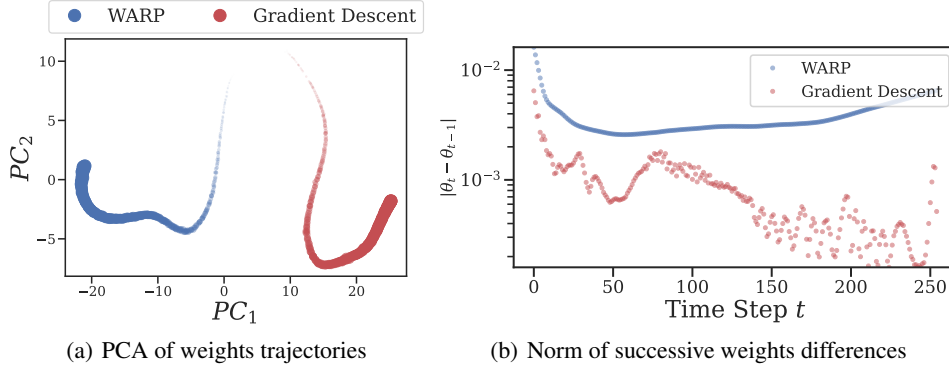


Figure 5: **(a)** Principal components of the weight-space of WARP vs. weight trajectory fitted via the Gradient Descent strategy on a single trajectory; **(b)** Norm of the difference between updates as we go through the time steps for WARP, and the gradient steps for Gradient Descent.

A.2 Training Algorithms

WARP's Recurrent Training Algorithm

Input: Training sequences $\{\mathbf{x}_t^i\}_{t \in \{0, \dots, T-1\}}^{i \in \{0, \dots, N-1\}}$

Output: Trained model parameters (A, B, ϕ)

Algorithm:

1. Initialize $A = I, B = \mathbf{0}$
2. **for** each training epoch **do**
3. **for** each batch of sequences **do**
4. **for** each sequence $\{\mathbf{x}_t^i\}_{t \in \{0, \dots, T-1\}}$ in batch **do**
5. Initialize $\theta_0 = \phi(\mathbf{x}_0)$
6. **for** $t = 1$ to $T - 1$ **do**
7. Update $\theta_t = A\theta_{t-1} + B(\mathbf{x}_t - \mathbf{x}_{t-1})$
8. Compute output $\mathbf{y}_t = \theta_t(\frac{t}{T-1})$
9. **end for**
10. Compute sequence loss \mathcal{L}^i
11. **end for**
12. Update parameters A, B, ϕ using gradient descent
13. **end for**
14. **end for**

Figure 6: Recurrent training algorithm for WARP in its non-AR form.

Recurrent Mode The recurrent training algorithm is illustrated in its non-AR setting in Figure 6. For the AR setting trained with teacher forcing, \mathbf{x}_t in line 7 is replaced, with probability $1 - p_{\text{forcing}}$, with a sample from $\mathcal{N}(\hat{\boldsymbol{\mu}}_t, \hat{\boldsymbol{\sigma}}_t^2)$ which is taken element-wise using the classic reparameterization trick as outlined in Section 2.3. The batch of sequences (lines 4 to 11) is computed in parallel using vectorization as per the implementation details below.

Convolutional Mode Like [Gu et al., 2021], WARP supports a convolutional training mode where the sequence of weights is computed efficiently using Fast-Fourier Transforms (FFTs) on modern hardware [Rush and Karamcheti, 2022] using Theorem 1. We use the Pythonic notation $\mathbf{u}_{0:T} \triangleq \{\mathbf{u}_t\}_{t=0}^{T-1} \in \mathbb{R}^{T \times D_u}$, and the \star to denote the convolution operation. The summarized convolutional training algorithm is provided in Figure 7.

Theorem 1 (Convolution Mode). *Assume $B \in \mathbb{R}^{D_\theta \times D_x}$ is a full row-rank matrix. There exists $\Delta \mathbf{x}_0 \in \mathbb{R}^{D_x}$ and a length- T kernel K such that $\theta_{0:T} = K \star \Delta \mathbf{x}_{0:T}$.*

Proof. It follows straightforwardly that the linear recurrence relation $\theta_t = A\theta_{t-1} + B\Delta \mathbf{x}_t$ can be unrolled as

$$\theta_t = A^t \theta_0 + \sum_{\ell=0}^{t-1} A^\ell B \Delta \mathbf{x}_{t-\ell}, \quad \forall t \in \{1, \dots, T-1\}. \quad (4)$$

Since B is of full row-rank, the mapping $\mathbf{u} \mapsto B\mathbf{u}$ is surjective, and $\exists \Delta \mathbf{x}_0 \in \mathbb{R}^{D_x}$ such that

$$\theta_0 = B\Delta \mathbf{x}_0. \quad (5)$$

Substituting this into (4), we get

$$\theta_t = \sum_{\ell=0}^t A^\ell B \Delta \mathbf{x}_{t-\ell}, \quad \forall t \in \{0, \dots, T-1\}, \quad (6)$$

from which the large kernel—the sequence of columns of the Kalman controllability matrix [Trélat, 2005]—is extracted:

$$K = (B, AB, A^2B, \dots, A^{T-1}B), \quad (7)$$

to form the relation

$$\theta_{0:T} = K \star \Delta \mathbf{x}_{0:T} \quad (8)$$

□

In practice, however, we find the assumptions of Theorem 1 too restrictive to be applicable. Indeed, with the weight-space typically larger than the input space, i.e. $D_\theta \gg D_x$, the mapping $\mathbf{u} \mapsto B\mathbf{u}$ is not *surjective*. For such cases, we leverage the initial network ϕ to enforce additional constraints into the learning process. Theorem 2 guarantees the existence of a suitable initial input difference $\Delta \mathbf{x}_0$ to use as input in the convolution (8).

Theorem 2 (Existence of an Initial Input Difference). *Fix ϕ as a locally linear operator with $B = \nabla \phi(\mathbf{x}_0)$, and assume $\ker \phi \neq \emptyset$. There exists $v \in \mathbb{R}^{D_x}$ such that $\Delta \mathbf{x}_0 = \mathbf{x}_0 - v$ and Equation (8) holds.*

Proof. The proof is straightforward by remarking that $\theta_0 = \phi(\mathbf{x}_0)$. Using Equation (5), we find that

$$\begin{aligned} \theta_0 &= B\Delta \mathbf{x}_0 \\ \Rightarrow \phi(\mathbf{x}_0) &= 0 + B\Delta \mathbf{x}_0 \end{aligned}$$

Since $\ker \phi \neq \emptyset$, $\exists v$ such that $\phi(v) = 0$, and since we've fixed $B = \nabla \phi(\mathbf{x}_0)$, this leads to

$$\phi(\mathbf{x}_0) = \phi(v) + \nabla \phi(\mathbf{x}_0) \Delta \mathbf{x}_0.$$

Since ϕ is locally linear, this relation can be identified with its unique first-order Taylor expansion near \mathbf{x}_0 , from which we identify $\mathbf{x}_0 = v + \Delta \mathbf{x}_0$; or equivalently $\Delta \mathbf{x}_0 = \mathbf{x}_0 - v$.

□

WARP’s Convolutional Training Algorithm

Input: Training sequences $\{\mathbf{x}_t^i\}_{t \in \{0, \dots, T-1\}}^{i \in \{0, \dots, N-1\}}$
Output: Trained model parameters (A, B, ϕ)

Algorithm:

1. Initialize $A = I, B = \mathbf{0}$
2. **for** each training epoch **do**
3. **for** each batch of sequences **do**
4. **for** each sequence $\{\mathbf{x}_t^i\}_{t \in \{0, \dots, T-1\}}$ in batch **do**
5. Initialize $\theta_0 = \phi(\mathbf{x}_0)$ and $\Delta \mathbf{x}_0$ (⊗ Equation (5) and Theorem 2)
6. Compute $\theta_{0:T} = K \star \Delta \mathbf{x}_{0:T}$ (⊗ Equation (8))
7. **for** $t = 1$ to $T - 1$ **do**
8. Compute output $\mathbf{y}_t = \theta_t(\frac{t}{T-1})$
9. **end for**
10. Compute sequence loss \mathcal{L}^i
11. **end for**
12. Update parameters A, B, ϕ using gradient descent
13. **end for**
14. **end for**

Figure 7: Convolutional training algorithm for WARP, where line 6 can be computed with (inverse) FFTs and the convolution theorem. All decoding sequence steps (lines 7-9), as well as the individual sequences (the batch from lines 4-11) are processed in parallel.

A.3 Implementation Details

The difference between a successful WARP training and a failure may lie in small implementation details. We recommend clipping several quantities to increase the chances of success.

Prediction Clipping During our training, we found it important to constrain the outputs of the root network to avoid divergence and blow-up. This can be achieved through a final activation applied to the mean component of the output, with e.g. *min-max* symmetric clipping:

$$\mathbf{x}_t \mapsto \max(\min(\mathbf{x}_t, d_{\text{lim}}), -d_{\text{lim}}),$$

with hyperparameter $d_{\text{lim}} > 0$. Another powerful approach which has demonstrated great success in the realm of Transformers is the *dynamic tanh* [Zhu et al., 2025] with learnable scalars a, b, α, β :

$$\mathbf{x}_t \mapsto \alpha \tanh\left(\frac{\mathbf{x}_t - b}{a}\right) + \beta,$$

with (a, α) initialized as the largest value encountered in the training datasets, and (b, β) both as zero. This ensures output scaling that is consistent in shape with the classical tanh activation.

Weight Clipping In some problems like MNIST, we found it not enough to constrain the root’s output within a certain bound, as the predictions kept diverging. In such cases, mechanisms like directly clipping the weights in between time steps provided an additional form of non-linearity helpful for the model. Our weight clipping strategy differs from traditional approaches discussed in continual learning contexts [Elsayed et al., 2024] as it does not consider initialization:

$$\theta_t = \text{clip}(\theta_t, -w_{\text{lim}}, w_{\text{lim}}),$$

where w_{lim} is a hyperparameter, and `clip` is a shorthand for *min-max* clipping as discussed above. This clipping operation serves as an implicit activation function in weight space, preventing unbounded growth in weight values and stabilizing training.

Gradient Clipping As customary with recurrent networks training with the backpropagation through time algorithm [Werbos, 1990], we observed the classical problem of exploding gradients [Zucchet and Orvieto, 2024], which was mitigated by clipping the gradient norms within a specific bound captured by $g_{\text{lim}} = 10^{-7}$.

B Datasets, Baselines & Metrics

B.1 Datasets

Table 4: Problems and their corresponding training datasets with specifications. Details about the UEA datasets are presented in Table 3 and not repeated here. The term (*varies*) indicates that further splits of the datasets were made.

PROBLEM	DATASET	# SAMPLES N	SEQ. LENGTH T	CONTEXT LENGTH L	# FEATURES D_x
2D Images	MNIST	60,000	784	(<i>varies</i>)	1
	Fashion MNIST	60,000	784	(<i>varies</i>)	1
	CelebA	162,770	1,024	(<i>varies</i>)	3
ETT	m1	34,369	192	96	7
	m2	34,369	192	96	7
	h1	8,449	192	96	7
	h2	8,449	192	96	7
Dynamical Systems	MSD	20,480	256	100	2
	MSD-Zero	20,480	256	100	2
	LV	15,000	256	100	2
	SINE	(<i>varies</i>)	16	1	1
	Spirals	10,000	64	64	2

We describe various datasets used in this paper. Our description delves into the details of pre-existing datasets and the data generation script of synthetic toy datasets. This section complements the summary we provided in Table 4.

Image Datasets Both MNIST [LeCun et al., 1998] and Fashion MNIST [Xiao et al., 2017] datasets were loaded using the well-known PyTorch interface [Paszke et al., 2017]. The values were then normalized so that pixel values ranged $[-1, 1]$. The CelebA dataset [Liu et al., 2015] was loaded using the API from [Nzoyem et al., 2024] itself inspired by [Zintgraf et al., 2019]. Training was performed on the train sets (see attributes in Table 4), with validation and testing on the predefined test sets.

Electricity Transformer Temperature (ETT) For the electricity data [Zhou et al., 2021], we further normalized the preprocessed data from TSLib to place all values in the range $[-1, 1]$ in order to facilitate learning dynamics. We did not use the predefined “test” set because of its 144 steps-long forecast window, which is much longer than the 96 steps all models saw during training⁷. Consequently, we used the “validation” set to evaluate our models as well as all the baselines.

University of East Anglia (UEA) On the UEA dataset [Bagnall et al., 2018], we follow the procedure from [Walker et al., 2024] and reuse the same dataset. (We note that this exact experimental protocol was recently observed in [Rusch and Rus, 2024]). We extracted the necessary scripts for reproducibility and provide them as part of our code under appropriate license.

Dynamical Systems Continuous autonomous dynamical systems can be conceptualized as multivariate time series governed by a deterministic vector field $(\mathbf{x}_\tau, p) \mapsto \dot{\mathbf{x}}_\tau$, with p encompassing physical parameters affecting the dynamics. Given an initial condition \mathbf{x}_0 , one can systematically simulate and subsample the trajectory $\mathbf{x}_{0:T}$. To complement our description in Section 3.2, we provide the vector field used for each dataset in Table 5. We summarize their physical parameter ranges in Table 6. All trajectories are obtained with SciPy’s ‘RK45’ adaptive time-stepping numerical integrator [Virtanen et al., 2020]. The five training data splits of the SINE are “Tiny”, “Small”, “Medium”, “Large”, “Huge”, with respectively 1, 10, 100, 1k, and 10k samples. All datasets are normalized and placed within the $[-1, 1]$ which is calculated using train set statistics. Comprehensive data generation scripts with physical parameters for all four datasets are provided in our code.

Spirals The Spirals dataset is an additional dynamical system dataset for binary classification tasks. The training data consists of 10,000 samples, where each sample is a spiral trajectory represented as a sequence of 64 2D points (x, y) coordinates). Half of the dataset contains clockwise spirals (labeled

⁷Forecasting experiments with inference beyond the training regime, i.e., $\tau > 1$, are reserved for future work.

Table 5: List of considered dynamical systems with their vector fields and/or flow maps.

DATASET	PHYSICAL PARAMETERS	VECTOR FIELD	FLOW MAP
Mass-Spring-Damper (MSD)	m, k, c	$\begin{cases} \dot{x}_1 = x_2 \\ \dot{x}_2 = -\frac{k}{m}x_1 - \frac{c}{m}x_2 \end{cases}$	Not used
Lotka-Volterra (LV)	$\alpha, \beta, \gamma, \delta$	$\begin{cases} \dot{x}_1 = \alpha x_1 - \beta x_1 x_2 \\ \dot{x}_2 = \delta x_1 x_2 - \gamma x_2 \end{cases}$	Non-closed form solution
Sine Curves (SINE)	φ	Not used	$x_1(t) = \sin(2\pi t + \varphi)$

Table 6: Parameter ranges of several dynamical systems for Train and Test datasets. Test set parameter ranges induce OoD trajectories, except for the SINE cases. The relative scale and broad range of parameters values for the MSD problem make this task extremely challenging.

DATASET	TRAIN PARAMETER RANGES	TEST PARAMETER RANGES
Mass-Spring-Damper (MSD)	$\begin{cases} m \in [0.02, 0.04] \\ k \in [4, 16] \\ c \in [0.01, 0.2] \end{cases}$	$\begin{cases} m \in [0.01, 0.05] \\ k \in [2, 18] \\ c \in [0.01, 0.3] \end{cases}$
Lotka-Volterra (LV)	$\begin{cases} \alpha \in [20, 50] \\ \beta \in [80, 120] \\ \gamma \in [80, 120] \\ \delta \in [20, 50] \end{cases}$	$\begin{cases} \alpha \in [10, 60] \\ \beta \in [70, 130] \\ \gamma \in [70, 130] \\ \delta \in [10, 60] \end{cases}$
Sine Curves (SINE)	$\varphi \in [-\pi/6, \pi/6]$	$\varphi \in [-\pi/6, \pi/6]$

as 0), while the other half contains counterclockwise spirals (labeled as 1). The spirals are generated using sine and cosine functions with random phase offsets, and the amplitude decreases with time to create the spiral effect. This dataset serves as a powerful test case for dynamics classification; it was inspired by [Kidger and Garcia, 2021]⁸, with a few samples visualized in Figure 8.

B.2 Baselines

All models are trained based on the same hyperparameter tuning protocol in order to ensure fair comparability.

Standard RNNs We consider two powerful RNN baselines including the Gated Recurrent Unit (GRU) [Cho et al., 2014] and the Long Short-Term Memory (LSTM) [Hochreiter and Schmidhuber, 1997]. Both are trained in recurrent AR mode for forecasting problems and recurrent non-AR mode for classification. Depending on the experiment, we vary their hidden size to match the total parameter count of WARP. The remainder of the experiment details such as training procedure are presented in Appendix C. We attach both implementations, using Equinox [Kidger and Garcia, 2021], to our code.

Time Series Transformer (TST) We consider the Time Series Transformer from HuggingFace [Jain, 2022]. This baseline provides a SoTA baseline, leveraging one of the most transformative sequence mixing processes to date: Attention. The specific model used was the *TimeSeriesTransformer-ForPrediction*, which adds a distribution head on top of the vanilla encoder-decoder Transformer [Vaswani et al., 2017]. This means that the model learns a distribution, from which we take the mean to be used for time-series forecasting. The next token prediction is obtained by randomly sampling a window of context length L plus prediction length $T - L$ from the target time series. This prediction window is subsequently masked for the next token prediction task.

Convolution Conditional Neural Process (ConvCNP) The ConvCNP [Gordon et al., 2020] is an encoder-based meta-learning approach which doesn’t require gradients in order to adapt to novel scenarios. The ConvCNP is trained for on-the-grid image completion with 100 random shots (time

⁸An example usage can be found at https://docs.kidger.site/diffrax/examples/neural_cde/

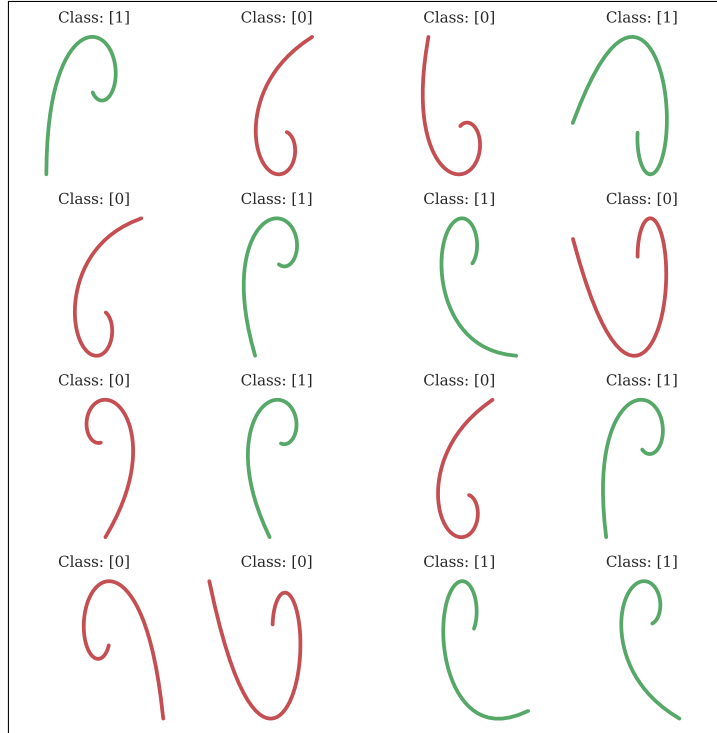


Figure 8: Visualization of a few samples of the Spirals datasets. For each sample, we plot the y and the x sequences of coordinates against each other to observe the (counter-)clockwise direction.

steps. We adapt its data loading process to allow the ConvCNP to operate on raster-scan-ordered pixels at test time.

Structured SSM (S4) We use the powerful Structured State Space Model S4 with the implementation of [Rush and Karamcheti, 2022]. We particularly apply it to the MNIST experiment, where the goal is to forecast a contiguous range of future predictions given a range of past contexts. To that end, we simply concatenate the entire context with a sequence of masks set to the length of the forecast window. This input is a single sequence of length T that is run through the deep S4 model, which maps to an output of length T . We then use the last $T - L$ tokens as the forecasted predictions.

Neural Controlled Differential Equation (NCDE) NCDEs or (Neural CDEs) [Kidger et al., 2020] provide a continuous-time framework for processing irregularly-sampled time series by interpreting the data as a continuous path. By using the path as a control for a neural differential equation, NCDEs can naturally handle missing data and irregular sampling. The continuous nature of NCDEs makes them a strong baseline exclusively for classification tasks.

Baselines for classification Mamba, S6, Log-CDE, NRDE, NCDE, LRU were all reported from [Walker et al., 2024], where we direct the reader for further details. We reused the results and the conclusion from that work, as was done by Rusch and Rus [2024].

B.3 Metrics

Bits Per Dimension (BPD) The (BPD) is used to evaluate the quality of generative models, particularly for images. It quantifies how many bits are needed on average to encode each dimension (e.g., pixel) of the data, with lower BPD values indicating a better model. The BPD is derived from the negative log-likelihood (NLL) of the data under the model’s predicted distribution. For a given ground truth pixel value y_t and its corresponding predicted mean \hat{y}_t and standard deviation $\hat{\sigma}_t$, the overall NLL over the image is calculated as:

$$\text{NLL} \triangleq \frac{1}{T} \sum_{t=0}^{T-1} \frac{1}{2} \log(2\pi\hat{\sigma}_t^2) + \frac{1}{2} \frac{(\mathbf{y}_t - \hat{\mathbf{y}}_t)^2}{\hat{\sigma}_t^2}.$$

The BPD is obtained by converting the NLL from natural units of information to bits:

$$\text{BPD} = \text{NLL} \times \log_2(e).$$

Mean Absolute Error (MAE) The MAE measures the average magnitude of the errors in a set of predictions. For a sequence of true values \mathbf{y}_t and predicted values $\hat{\mathbf{y}}_t$, the MAE is given by:

$$\text{MAE} \triangleq \frac{1}{T} \sum_{t=0}^{T-1} |\mathbf{y}_t - \hat{\mathbf{y}}_t|.$$

Mean Absolute Percentage Error (MAPE) The Mean Absolute Percentage Error (MAPE) expresses the average absolute percent error. The MAPE is given in percentage points by:

$$\text{MAPE} \triangleq \frac{100}{T} \sum_{t=0}^{T-1} \left| \frac{\mathbf{y}_t - \hat{\mathbf{y}}_t}{\mathbf{y}_t} \right|.$$

C Experimental Details

We begin this section by sharing experimental details shared across all problems. Subsequent subsections will delve into the specifics of each completion, forecasting or classification problem.

WARP setup. Although specific details may vary depending on the problem, the root network is consistently chosen as a MLP for all problem sets in this paper. Given the quadratic memory cost $O(D_\theta^2)$, we can vary its layers to balance batch size with capacity. Image completion and forecasting problems use the ReLU activation [Agarap, 2018], while smooth dynamical system reconstruction use the Swish [Ramachandran et al., 2017]. Complete details on the root network are given in Table 7. The initial hypernetwork ϕ —used for all problems except Image Completion, MSD, and LV—is made up of two hidden layers of width $h_{\text{in}}/3 + 2h_{\text{out}}/3$ and $2h_{\text{in}}/3 + h_{\text{out}}/3$ neurons, respectively. The positive integers h_{in} and $h_{\text{out}} = D_\theta$ are the number of input and output neurons respectively.

WARP-Phys setup. For the SINE experiment, the root network predicts the phase $\hat{\varphi}$ to feed into the sinusoid $\tau \mapsto \sin(2\pi\tau + \hat{\varphi})$. For the challenging MSD and MSD-Zero problems, we embed knowledge of the general analytical solution and the initial condition with $\tau \mapsto E(\tau)\mathbf{x}_0$, where $E(\cdot) \in \mathbb{R}^{2 \times 2}$ with its four coefficients predicted by the root network, and \mathbf{x}_0 is known throughout. $E(\tau)$ is viewed as the exponential of τA , where A is the constant matrix characterizing the mass-spring-damper dynamics: $A = \begin{pmatrix} 0 & 1 \\ -k/m & -c/m \end{pmatrix}$ [Nzoyem and Labbe, 2021]; its poor conditioning — a consequence of the large parameter scales and ranges detailed in Table 6 — would destabilize the training if A was directly learned. We note that stronger levels of physics may be embedded into the root network: predicting rescaled time-invariant constants (m, k, c) , parameterizing the signal as damped sinusoids, eigen-decomposition, etc. The physics-informed strategy we present is the one that produced the biggest improvement over WARP in our experiments.

Optimization & Core baselines. Our WARP framework (along with our custom GRU, LSTM, ConvCNP, and Neural CDE) is implemented with the JAX framework [Bradbury et al., 2018] and its ecosystem: Equinox for neural network definitions [Kidger and Garcia, 2021], and Optax for optimization [DeepMind et al., 2020]. We use the AdaBelief optimizer [Zhuang et al., 2020], and we clip the gradient norm with $g_{\text{lim}} = 10^{-7}$. We apply the “reduce on plateau” rule where the learning rate is divided by 2 if the average loss⁹ doesn’t evolve after 20 epochs. For most problems, we set the initial learning rate at 10^{-5} . All GRU and LSTM models have a single layer to match WARP. We tweak their hidden size rather than the number of layers in order to increase or reduce parameter count, thus keeping in check the complexity of the models under consideration.

TST and S4 baselines setup. As for the TST model for forecasting, it is implemented in PyTorch [Paszke et al., 2017] and uses the AdamW optimizer with a constant learning rate of 6×10^{-4} , beta values of 0.9 and 0.95 and weight decay coefficient of 10^{-1} . For the S4 model, we used 6 layers, each with a hidden state of size 512, a batch size of 50, a learning rate of 10^{-3} , and the traditional weight decay with coefficient 0.05. Like [Rush and Karamcheti, 2022], we used prenormalization, but we did not use dropout. These hyperparameters were selected based on the validation set when available, and the test set if not (e.g., all synthetic toy problems).

Hardware. The WARP, GRU, LSTM, ConvCNP and S4 models are run on a workstation fitted with a RTX 4080 GPU with a memory capacity of 16 GB. The TST was trained on a RTX 3090 GPU with 24 GB memory.

C.1 Image Completion

On these problems, since trained with the NLL loss from Equation (3), we use a dynamic tanh activation function on the mean prediction, with (a, b, α, β) initialized as $(1, 0, 1, 0)$. Only experiments run on MNIST and Fashion MNIST use weight clipping, while CelebA does not¹⁰. For CelebA, we use $\sigma_{\text{lim}} = 10^{-4}$ (see Equation (2)) while we find the unusually large $\sigma_{\text{lim}} = 0.5$ suitable for MNIST and Fashion MNIST. We compare WARP to the MNIST baselines roughly at the same parameter counts: GRU (1.694 M), LSTM (1.696 M), S4 (1.717 M), and WARP (1.687 M). We train for 200

⁹The average being calculated over 50 iterations.

¹⁰Apart from (Fashion) MNIST, no other problem in this work used weight clipping.

Table 7: Root MLP configurations for each dataset for each problem.

PROBLEM	DATASET	WIDTH	DEPTH	ACT. FUNCTION
2D Images	MNIST	24	3	ReLU
	Fashion MNIST	24	3	ReLU
	CelebA	24	3	ReLU
ETT	m1	148	1	ReLU
	m2	148	1	ReLU
	h1	148	1	ReLU
	h2	148	1	ReLU
Dynamical Systems	MSD	48	3	Swish
	MSD-Zero	48	3	Swish
	LV	48	3	Swish
	SINE	48	3	Swish
	Spirals	24	1	Swish
UEA	Worms	128	1	ReLU
	SCP1	48	2	ReLU
	SCP2	48	2	ReLU
	Ethanol	32	2	ReLU
	Heartbeat	72	2	ReLU
	Motor	32	2	ReLU

Table 8: Size of the hidden state in standard RNNs for each dataset.

PROBLEM	DATASET	LSTM HIDDEN UNITS	GRU HIDDEN UNITS
2D Image	MNIST	750	750
	Fashion MNIST	650	750
	CelebA	700	825
ETT	m1	920	920
	m2	920	920
	h1	920	920
	h2	920	920
Dynamical Systems	MSD	2450	2850
	MSD-Zero	2450	2850
	LV	2450	2850
	SINE	2280	2280

and 250 epochs in batches of 640 and 1256 for (Fashion) MNIST and CelebA respectively. We apply the recurrent AR mode with $p_{\text{forcing}} = 0.15$, while directly feeding the mean prediction back into the recurrence (i.e., the reparameterization trick is disabled both during training and inference).

C.2 Image classification

For this task, we use the same hyperparameters as the MNIST task described above, with the only difference that the training is now performed in recurrent non-AR mode.

C.3 Energy forecasting

For these experiments, all models share identical architectures across the four datasets (ETT-h1, ETT-h2, ETT-m1, ETT-m2). The learning rate differs between hourly and minute-level datasets: 10^{-5} for h1/h2 and 10^{-4} for m1/m2. For hourly datasets, we train for 500 epochs, while minute-level datasets require only 250 epochs (corresponding to roughly 1.5 hours of training). All models are trained with batch size 3600 in autoregressive mode with stochastic sampling (non-AR), and $p_{\text{forcing}} = 0.25$. No final activation is applied to the root network’s mean output, while the typical positivity-enforcing from Equation (2) is applied to the standard deviation with $\sigma_{\text{lim}} = 10^{-4}$.

C.4 Dynamical System Reconstruction

For the dynamical system reconstruction tasks, since uncertainties are not required, models are trained without NLL loss (i.e., with the MSE loss defined in Equation (3)). Consistent across all dynamical system experiments, no weight clipping is employed, and the predictions are enforced in the range $[-1, 1]$ with a unit-initialized dynamic tanh. All losses are computed on the normalized test set.

Mass-Spring-Damper (MSD and MSD-Zero) For both the MSD and its MSD-Zero variant, the experimental setup is largely identical. A learning rate of 10^{-5} is used. Training proceeds for 1000 epochs using a batch size of 1024. WARP, GRU, and LSTM models are trained in an auto-regressive mode with a teacher forcing probability $p_{\text{forcing}} = 0.25$.

Lotka-Volterra (LV) The LV experiment is performed for 1500 epochs with a batch size of 1024. Training is conducted with a teacher forcing probability $p_{\text{forcing}} = 1.0$, meaning the model is always fed the ground truth inputs during training. This is because this is a memorization task, and the goal is for the model to predict the next token *knowing* the previous one. LSTM and GRU use the same hyperparameters, except with hidden states of sizes 2450 and 2850 respectively (see Table 8).

Sine Curves (SINE) Across the various SINE datasets (Tiny, Small, Medium, Large, Huge), a consistent configuration is maintained. The learning rate is set to 10^{-5} . Models are trained for 1000 epochs in a single batch (as large as 10000 on Huge). Similar to MSD, training is autoregressive with $p_{\text{forcing}} = 0.25$. No final activation is applied to the root network’s mean output. The inference process for SINE datasets begins with a very short context, of just 1 time step.

C.5 Time Series Classification

For time series classification tasks, encompassing both the UEA datasets and the Spirals dataset, models are consistently trained in the non-AR mode, with the categorical cross-entropy loss. Across all these classification experiments, root weight are evolved without weight clipping, and no dynamic tanh activation is applied to their final outputs. Key training hyperparameters exhibit some variation across these diverse datasets: the learning rate is 10^{-5} for the Spirals dataset and most UEA datasets (e.g., Ethanol, Heartbeat, Motor, SCP1, SCP2), with the Worms dataset being an exception at 10^{-6} . The number of training epochs varies widely, ranging from 800 for the Worms dataset, 4000 for Spirals, up to 6500 for the Ethanol UEA dataset, with other UEA datasets generally trained for several thousand epochs. Given our limitation of 16GB available VRAM memory, batch sizes also differ significantly; for instance, the Worms dataset uses a batch size of 40, other UEA datasets use batch sizes typically in the hundreds (from approximately 280 to 560), and the Spirals dataset employs a large batch size of 10000. Regarding data preprocessing, input data normalization is applied for several UEA datasets (specifically Ethanol, Heartbeat, SCP1, and SCP2), but it is not used for others like EigenWorms and MotorImagery, nor is it required for the Spirals dataset.

D Additional Results

D.1 2D Image Experiments

Similar to MNIST image completion, we train WARP, LSTM and GRU to generate items of clothing (Fashion MNIST). The results, presented in Table 9 confirm the potency of our framework, as previously evoked in Section 3.1. We perform an additional classification on the sequential MNIST dataset, where we observe a 99.93% accuracy on the subsampled grayscale images in $\mathbb{R}^{14 \times 14 \times 1}$.

Table 9: Best test-set MSEs and BPDs on Fashion MNIST across 3 runs with different seeds.

METHOD	MSE	BPD
GRU	0.078	0.66
LSTM	0.082	0.73
WARP	0.064	0.59

Table 10: Best accuracies and wall time comparison for Spirals classification across 3 runs.

METHOD	ACCURACY (%)	WALL TIME / EPOCH (SECS)
Neural CDE	100.0	0.12
WARP	99.96	0.41

D.2 Spirals & Neural CDEs

Table 10 reveals several limitations of WARP on the toy Spirals dataset originally introduced to test Neural CDEs [Kidger, 2022]. We find that at the same parameter count, WARP not only struggles to achieve 100% accuracy, but is also roughly $4\times$ slower, despite being implemented in the same conditions as the Neural CDE.

D.3 Dynamics Reconstruction

As mentioned in Figure 3(b), WARP uses a diagonal readout matrix $\theta_t(\tau)$ to self-decode the hidden states. This implies that post training, the weights θ_t and the time $\tau = t/(T - 1)$ should be correlated. We confirm this hypothesis by plotting the correlation coefficient between the vector $\theta_{0:T}$ and all time points across all samples in the test set. We observe a strong either positive or negative correlation between the two quantities (see Figure 9).

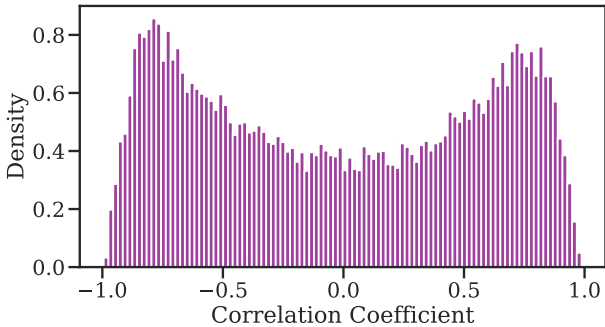


Figure 9: Correlation between the root network’s weights θ_t and the time τ on the MSD problem; indicating strong linear dependence between the two.

D.4 Extended Ablation Insights

We provide quantitative results for the ablation studies described in Section 3.4. Figures and Tables in this section are captioned with the corresponding paragraph title in Section 3.4.

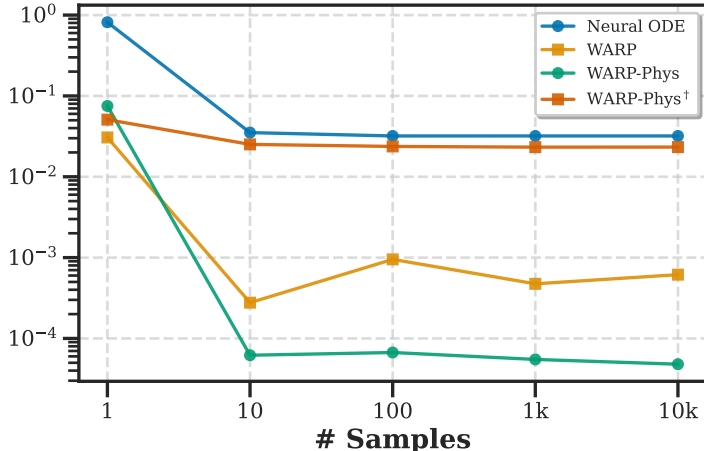


Figure 10: **Eliminating the root network** — Test-set MSEs on the SINE problem. The omission of θ_t in favor of directly fitting φ (which we call WARP-Phys[†]) results in a catastrophic degradation in model expressivity. Performance is almost as bad as the Neural ODE analyzed in Figure 4.

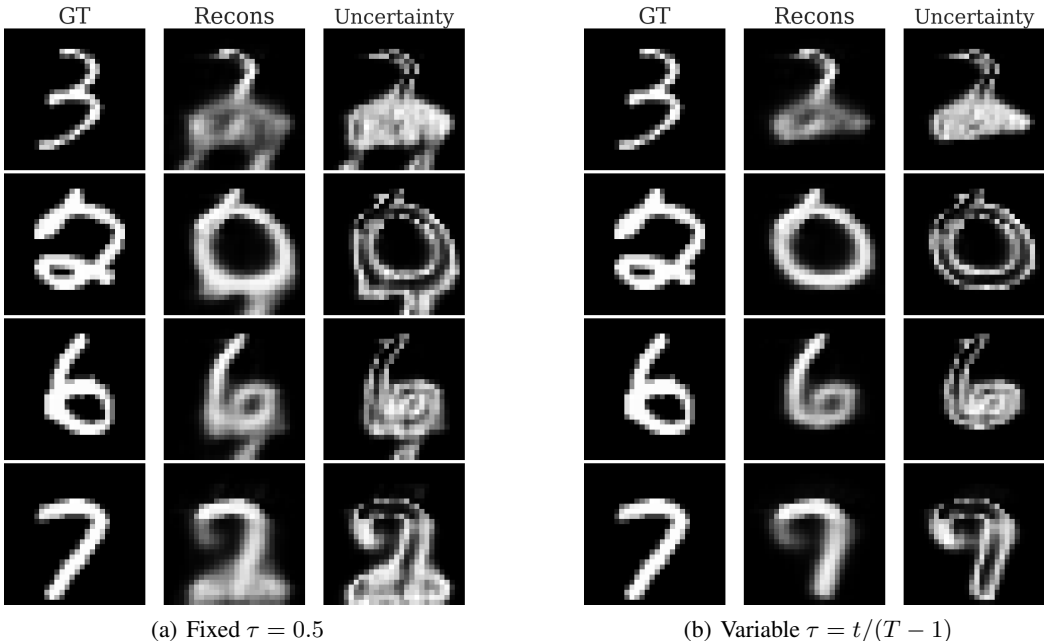


Figure 11: **Root network evaluation** — When we fix the evaluation point τ , we observe mild degradation in the qualitative results. While these figures are shown for MNIST with $L = 300$, the behavior is observed across problems, including dynamical systems like MSD (see Figure 3(b)). **GT** stands for the Ground Truth, **Recons** is for the Reconstruction/Completion, and **Uncertainty** is the model-outputted standard deviation.

Table 11: **Initial network configuration** — Empirical investigations reveal that sidestepping ϕ in favor of directly learning θ_0 curtails the model performance on complex synthetic benchmarks, such as MSD-Zero, and on real-world datasets, including ETTm1.

PROBLEM	WITH ϕ	WITH θ_0
MSD-Zero	0.32	1.02
ETTm1	0.02	1.25

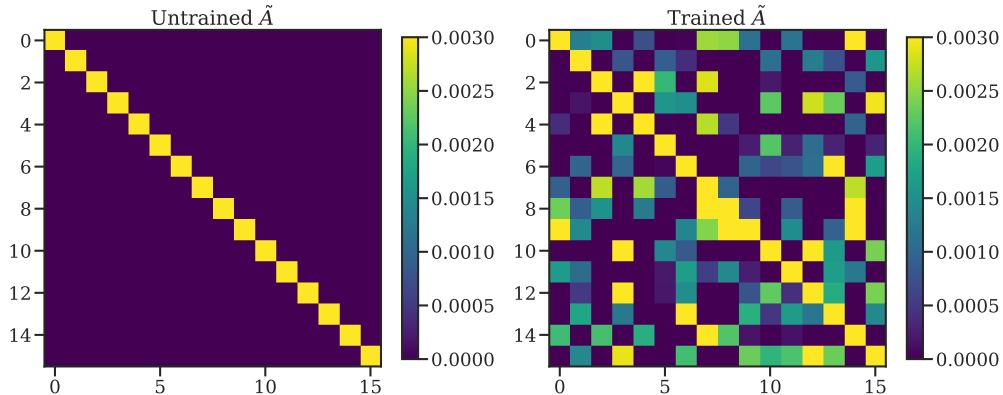


Figure 12: **Dense state transitions & Channel mixing** — Attempts to replace $A \in \mathbb{R}^{D_\theta \times D_\theta}$ with either a diagonal or a low-rank approximation \tilde{A} result in less expressive models. We observe here a low-rank $\tilde{A} \in \mathbb{R}^{16 \times 16}$ on the ETTm1 problem, such that $A = P\tilde{A}Q$, with all quantities in the right-hand side learnable.

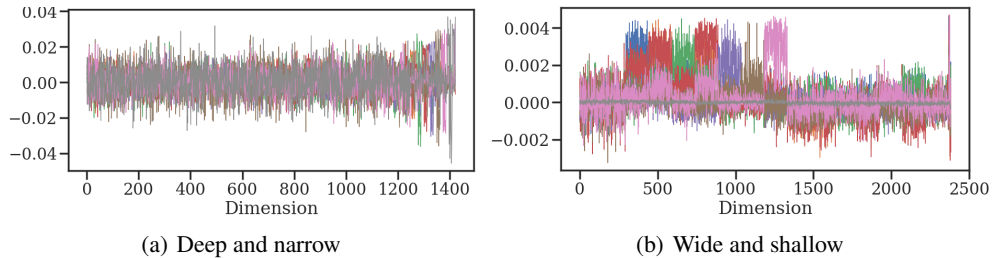


Figure 13: **Varying the root network** — If the root network is deep (Right), the last layer’s weights get larger compared to earlier layers. To make sure that all neurons are equally used, one could opt for the wide and shallow architecture (Left). This is shown for the electricity ETTm1 problem, and we remark that our recommendation doesn’t consider expressivity.

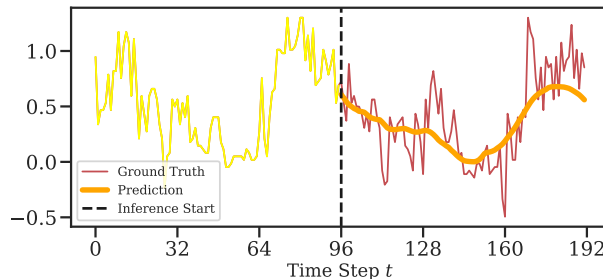


Figure 14: **Ablation of the reparameterization trick** — On the electricity problems, if stochastic sampling during training is not used, the model only predicts the mean of the distribution, thereby ignoring high-frequency components or noise in the signal. Here this is illustrated with a prediction on the ETTm1 test split.

E Visualizations

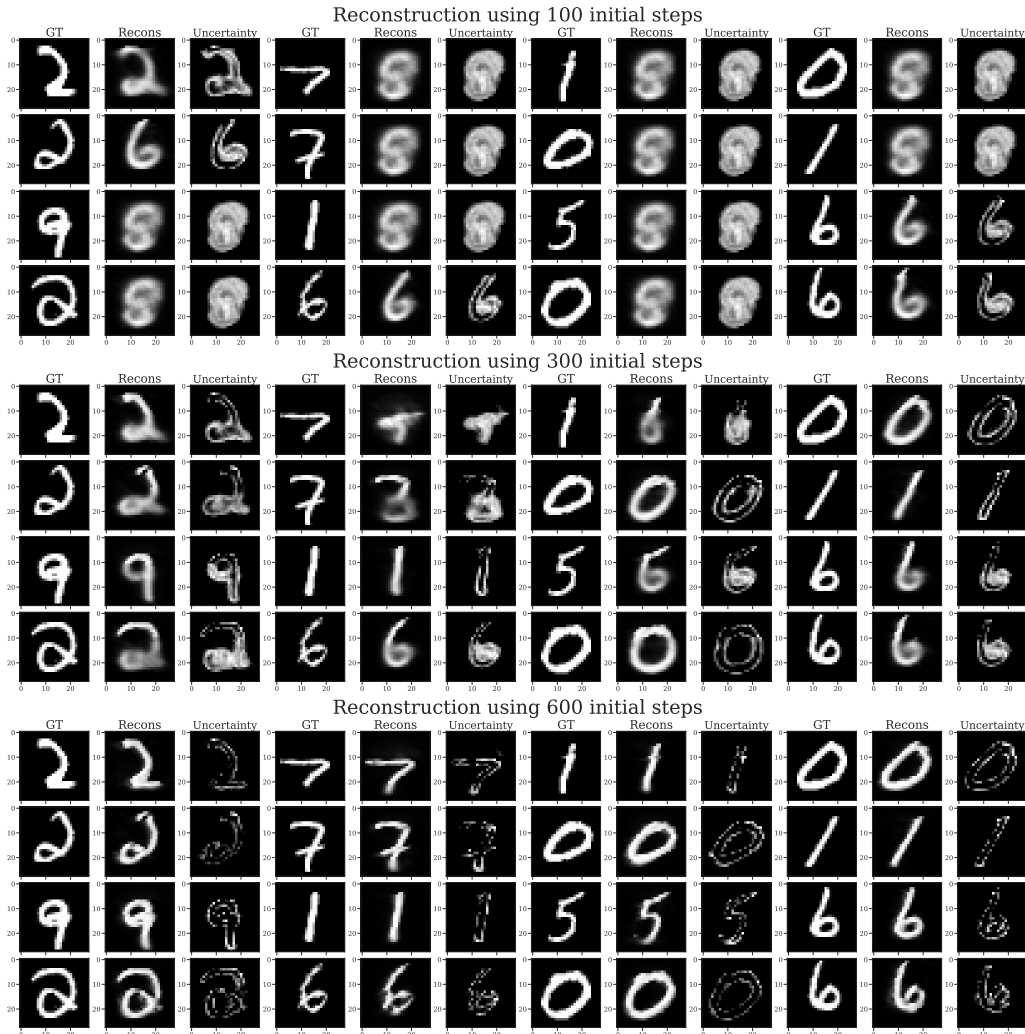


Figure 15: Completed images from the MNIST test set using WARP. The same set of images is shown across three settings: **(Top)** $L = 100$, **(Middle)** $L = 300$, **(Bottom)** $L = 600$. Along the columns, we show 4 groups of results, each with Ground Truth (GT), Reconstruction (Recons), and Uncertainty, resulting in 12 total columns. As our model sees more steps, its forecasting improves and its uncertainty decreases.

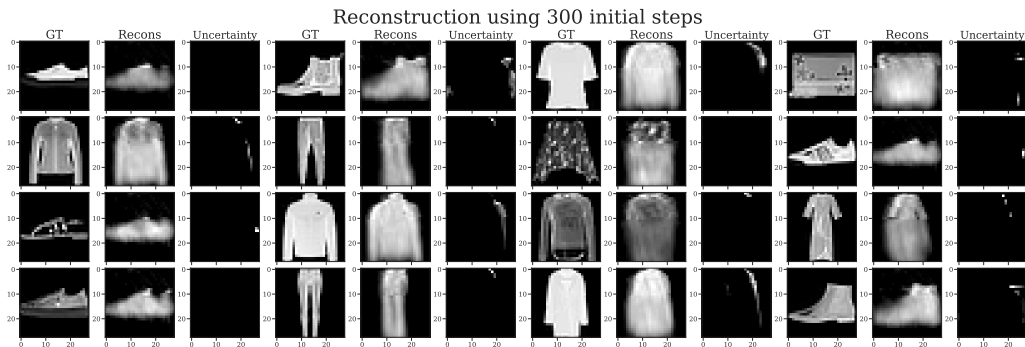


Figure 16: Completed images from the Fashion MNIST test set using WARP.



Figure 17: Completed images from the CelebA test set using WARP at various context lengths.



Figure 18: Completed images using WARP on the CelebA test set at high-resolution, illustrating the failure mode of limitation with long-range dependencies, e.g. when $T = 64 \times 64 = 4,096$.

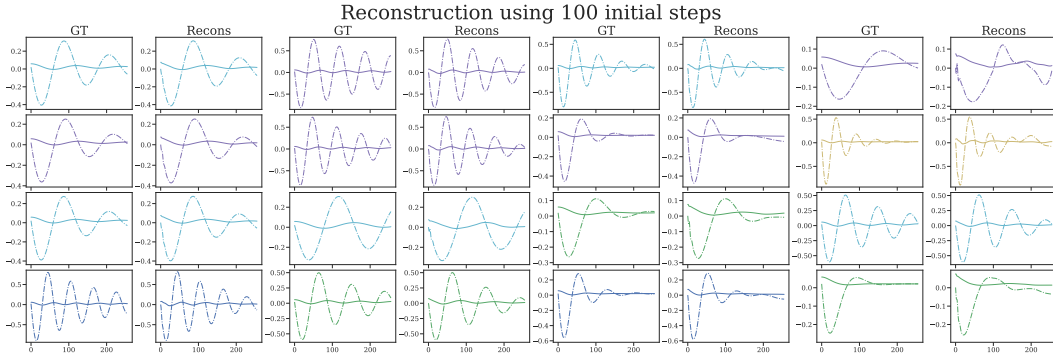


Figure 19: Completed sequences from the MSD test set using WARP.

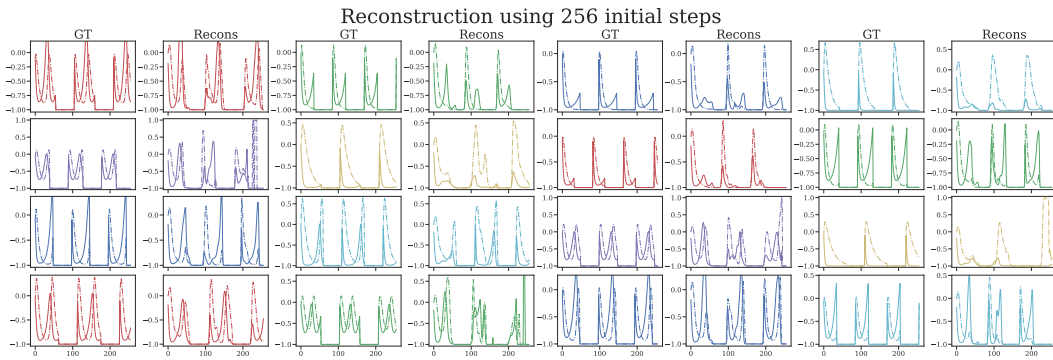


Figure 20: Completed sequences from the Lotka test set using WARP.

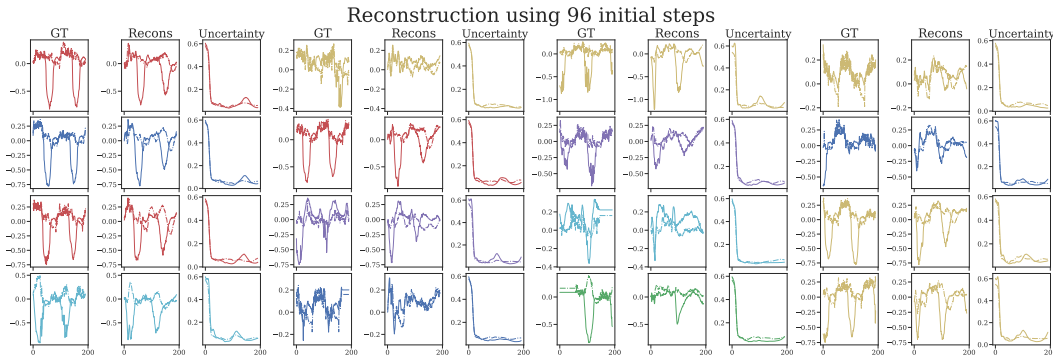


Figure 21: Completed time series from the ETTm1 test set using WARP.